

1 Main Manuscript for

2 A G-quadruplex-binding platinum complex induces cancer mitochondrial dysfunction *in* 3 *vitro* and *in vivo* independently of ROS induction

4 Keli Kuang^{a1}, Chunyan Li^{a1}, Fatlinda Maksut^{b,c}, Deepanjan Ghosh^{b,c}, Robin Vinck^d, Maoling
5 Wang^a, Joël Poupon^e, Run Xiang^f, Wen Li^g, Fei Li^a, Zhu Wang^a, Junrong Du^a, Marie-Paule
6 Teulade-Fichou^{b,c}, Gilles Gasser^d, Sophie Bombard^{b,c*} and Tao Jia^{a,b,c*}

8 a Key Laboratory of Drug-Targeting and Drug Delivery System of the Education Ministry and
9 Sichuan Province, Sichuan Engineering Laboratory for Plant-Sourced Drug and Sichuan
10 Research Center for Drug Precision Industrial Technology, West China School of Pharmacy,
11 Sichuan University, Chengdu 610041, China.

12 b CNRS-UMR9187, INSERM U1196, PSL-Research University, 91405 Orsay, France

13 c CNRS-UMR9187, INSERM U1196, Université Paris Saclay, 91405 Orsay, France

14 d Chimie ParisTech, PSL University, CNRS, Institute of Chemistry for Life and Health
15 Sciences, Laboratory for Inorganic Chemical Biology, F-75005 Paris, France.

16 e Hôpital Lariboisière (AP-HP), Laboratoire de Toxicologie Biologique, 2 rue Ambroise Paré,
17 75475 Paris, France

18 f Department of Thoracic Surgery, Sichuan Clinical Research Center for Cancer, Sichuan
19 Cancer Hospital & Institute, Sichuan Cancer Center, Affiliated Cancer Hospital of University
20 of Electronic Science and Technology of China, Chengdu, China.

21 g Department of Medical Oncology, Cancer Center, West China Hospital, Sichuan University,
22 Chengdu, China

23 Keli Kuang¹ and Chunyan Li¹ are considered joint first author.

24 *Corresponding author:

25 Tao Jia* Email: taojia86@scu.edu.cn;

26 Sophie Bombard* Email: Sophie.bombard@curie.fr

27 **Author Contributions:** S.B. and T.J. designed research; K.K., C.L., F.M., D.G., R.V., M.W., J.P.,
28 F.L., Z. W., S.B. and T.J. performed research; K.K., C.L., R.X., W.L., J.D., S.B. and T.J. analyzed
29 data; M.T., G.G., S.B. and T.J. wrote the paper.

31 **Competing Interest Statement:** The authors declare no competing interest.

33 **Keywords:** G4, Platinum complex, Mitochondrial genome, Mito-Nuclear Interactions, ROS,
34 chemotherapy

35 **This PDF file includes:**

36 Main Text
37 Figures 1 to 7
38
39
40
41
42

43 **Abstract**

44 G-quadruplex DNA (G4) is a non-canonical structure forming in guanine-rich regions, which play a
45 vital role in cancer biology and are now being acknowledged in both nuclear and mitochondrial (mt)
46 genome. However, the impact of G4-based targeted therapy on both nuclear and mt genome,
47 affecting mt function and its underlying mechanisms remain largely unexplored. Here, we first
48 demonstrated that the G4-binding platinum(II) complex, Pt-tpty, shows a highest accumulation in
49 the mitochondria of A2780 cancer cells as compared with two other platinum(II) complexes with
50 no/weak G4-binding properties, Pt-tpy and cisplatin. Pt-tpty significantly induces deletion, copy
51 number reduction and transcription inhibition of mt DNA, and it hinders the translation of mt
52 proteins. Functional study shows that Pt-tpty induces a potent mt dysfunction indicated by a high
53 reduction of mt membrane potential, oxygen consumption rate and ATP synthesis, as well as toxic
54 mt morphology switching, but without reactive oxygen species (ROS) induction. Mechanistic study
55 by RNA-seq, Chip-seq and CUT-RUN shows Pt-tpty impairs most nuclear-encoded mt ribosome
56 genes' transcription initiation through dampening the recruiting of TAF1 and NELFB to their
57 promoter, which are highly enriched in G4 forming sequences. *In vivo* studies on a A2780 tumor
58 xenograft mouse model suggest Pt-tpty's efficient anti-tumor effects, causing substantial disruption
59 in mt genome function, while exhibiting less side effects compared to cisplatin. Overall, this study
60 presents the first evidence that a G4-binding platinum(II) complex can harm cancer cell
61 mitochondria potently without inducing ROS activity, potentially reducing side effects that shows
62 promise in developing safer and effective platinum-based G4-binding molecules in cancer therapy.

63 **Significance Statement**

64 Despite molecules interacting with G4s have been intensively investigated as cancer therapeutics,
65 to explore potential of G4s in disturbing mitochondrial function for anti-cancer from both nucleus
66 and mitochondrial genome is almost neglected. Our research sheds light on this unexplored area
67 by introducing a G4-binding platinum(II) complex. Pt-tpty induces strong disturbance to
68 mitochondrial function *in vitro* and *in vivo* without ROS production, which is related to direct and
69 highly accumulating in mitochondria and indirectly inhibiting nuclear-encoded mitochondrial
70 ribosome gene expression by impairing the recruitment of transcription and elongation factors to
71 G4-rich regions. This unique property enhances its safety profile while delivering effective anti-
72 cancer benefits, offering the prospect of developing safer and more effective platinum-based
73 compounds targeting G4 structures in cancer therapy.

74

75 **Three Major findings:**

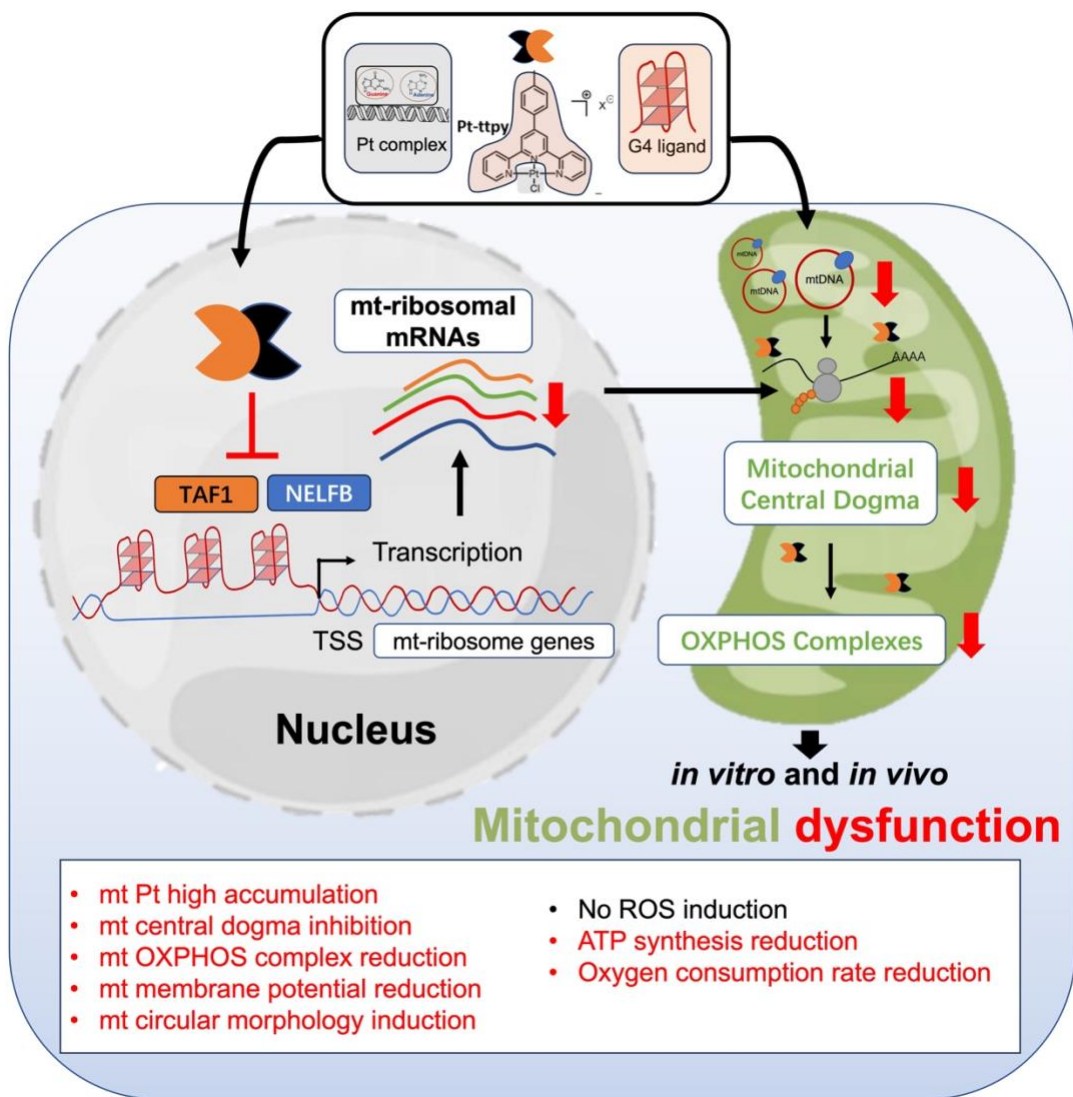
- 76 1. Pt-tpty demonstrates a substantial disruption to the mitochondrial genome function through a
77 direct effect on mitochondria and an indirect effect based on broad inhibition of G4-enriched
78 nuclear-encoded mt ribosome genes expression, spanning from mt DNA replication to its
79 translation *in vitro* and *in vivo*.
80
- 81 2. Pt-tpty displays effective anti-cancer benefits with improved safety, which can be attributed to
82 its induction of significant disruption in mitochondrial function without generation of reactive
83 oxygen species (ROS), thus reducing oxidative stress-related side effects commonly
84 associated with platinum complexes treatments, including cisplatin.
85
- 86 3. We provided first evidence that most of mt ribosome genes are highly enriched in G4 structures
87 in their promoter regions and thus are the targets of Pt-tpty that inhibits their expression through

88 dampening the recruitment of TAF1 and NELFB to G4 in nuclear DNA ultimately leading to the
89 induction of mt dysfunction.

90

91

92 **Graphic Abstract:**



93

94

95

96

97 **Main Text**

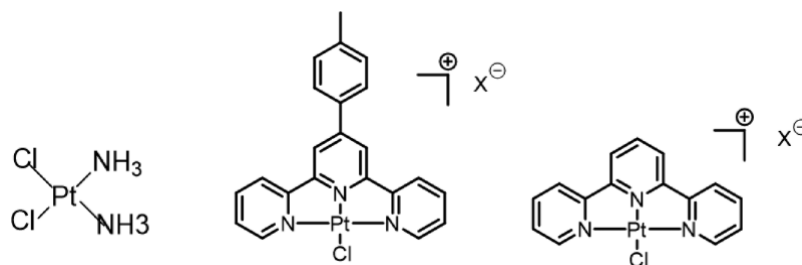
98

99 **Introduction**

100 G-quadruplex(G4) structures are non-canonical unique secondary four-stranded nucleic acids
101 structures folded in guanine-rich repetitive DNA or RNA sequences. They consist in the stacking of
102 guanine tetramers linked together by Hoogsteen hydrogen bonding, that are stabilized via π - π
103 interactions and monovalent cations (1) (2). The human genome contains about 350,000-600,000
104 potential G4 sequences by computer prediction (3) (4). Analysis of *in vitro* polymerase stop assays
105 revealed approximately 700,000 G4 structures (5), however, when employing the G4 ChIP-seq
106 assay, the frequency of G4s in human chromatin decreases significantly to be roughly 10,000 (6).
107 G4 structures have been extensively studied in nuclear DNA, mainly clustered in key regions of the
108 genome: telomeres, gene promoters and DNA replication start points (7) (8). Recent emerging
109 evidence emphasized the G4 presence in mitochondrial DNA (mt DNA) as well (9) (10) (11).
110 Prediction by the G4 Hunter algorithm revealed that the complete genome of a mitochondrion (16.6
111 kb) has approximately 96 G4s (4). Given the regulatory potential of G4 structures in mitochondrial
112 processes and their involvement in cancer, targeting G4 structures would have therapeutic
113 implications (12).

114 Mitochondria are specialized organelles that are at the heart of energy production (ATP) through
115 the oxidative phosphorylation (OXPHOS) pathways and serves as centers of cellular signaling and
116 apoptosis. They possess their own genome that codes notably for RNAs that encode 13 of the
117 protein subunits of OXPHOS complex, the other mitochondrial proteins being encoded by nuclear
118 genes. Mt DNA can be replicated independently of nuclear DNA and G4 structures in mt DNA are
119 closely related to its own replication and transcription (1) (13). Small molecules that can stabilize
120 G4 structures have been extensively explored as potential therapeutic agents for cancer (14-20).
121 Some evidence indicated that, in addition to target G4 structures in genomic DNA and RNA, they
122 could also target G4 structures in mt DNA. Notably the G4-ligand, RHPS4, interferes with
123 mitochondrial function through perturbation of mitochondrial genome replication, transcription
124 processivity, and respiratory function in mouse embryonic fibroblast cells (21). G4 structures are
125 present in both nuclear and mt genome, hence, to explore the potential of G4 structures in the
126 regulation of mitochondrial function for anti-cancer, investigation at both nuclear and mt genome
127 level is warranted, especially when exploring the use of G4 ligands.

128 We have previously reported on the tolyl-terpyridin-platinum complex (Pt-tpty) (Scheme 1) that
129 stabilizes G4s *in vitro* preferentially to duplex DNA through stacking to external G-tetrads (22, 23).
130 This compound is also able to efficiently trap G4s covalently by direct coordination to loop bases
131 (24, 25). Our previous cellular and molecular mechanism studies indicate that Pt-tpty binds
132 covalently to telomeric DNA *in cellulo* (26), inducing chromosome loss and ultrafine bridges
133 formation, resulting in telomeric DNA damage and telomere deprotection (27, 28), by inducing DNA
134 damage preferentially at G- and A-rich regions, displaying potent anti-tumor activity.



135

136 Scheme 1: Chemical structures of cisplatin (CisPt), Pt-ttpy and its terpyridine analogue Pt-tpy

137 In this study, we first demonstrated that Pt-ttpy exhibits strong disruption in mitochondrial function
 138 which is unrelated to the induction of reactive oxygen species (ROS). mt dysfunction was induced
 139 by G4 targeting in both nuclear and likely in mitochondrial genome as an alternative mechanism
 140 underlying the anti-tumor activity of Pt-ttpy by *in vitro* and *in vivo* studies. Secondly, we showed
 141 that Pt-ttpy displays effective anti-cancer benefits with relative improved safety, which can be
 142 attributed to its induction of mt dysfunction without production of ROS, thus reducing treatment-
 143 related side effects commonly associated with platinum complexes, e.g. cisplatin. Lastly, we
 144 provided first evidence that most mt ribosome genes that are highly enriched in G4 structures in
 145 their promoter regions, are the targets of Pt-ttpy. The latter inhibits their gene expression through
 146 dampening the recruitment of TAF1 and NELFB to their corresponding promoters in nuclear DNA
 147 that ultimately leads to induction of mt dysfunction. These findings lead to the promise for
 148 developing G4-binding platinum-based compounds with improved safety profiles as well as
 149 effective anti-cancer benefits.

150 Results

151 **Pt-ttpy shows significant highest accumulation within mitochondria, accompanied by a**
 152 **pronounced disturbance toward the Mitochondrial genome.**

153 Our previous work showed that the G4-binding Pt-ttpy complex and its terpyridine counterpart Pt-
 154 tpy as well as cisplatin (CisPt), the two latter having no to low affinity for G4, accumulate in cells
 155 and bind to genomic DNA in a time- and dose- dependent manner in ovarian cancer cells A2780
 156 (see Scheme 1 for structures of compounds). At iso-effect concentrations that achieve an 80%
 157 inhibition of cell proliferation over a 96-hour treatment period, there is a marked higher
 158 accumulation of Pt-ttpy in cells. This increase is observed alongside a similar level of genomic DNA
 159 binding efficiency with the occurrence of DNA damage among all the three Pt complexes, indicated
 160 in scheme 1 (28). Since some G4-binding ligands were shown to accumulate in mitochondria (mt)
 161 (21) as well as some platinum complexes (29), we hypothesized, due to the high cellular uptake of
 162 Pt-ttpy, that mitochondria could be a privileged target of Pt-ttpy. We therefore quantified the
 163 distribution of the three platinum complexes at iso-effect doses that are their respective IC_{80}
 164 concentration after 96 hours treatment in the ovarian cancer cell line A2780 cells using the ICP-MS
 165 method, in whole cells, in mitochondria and their fraction bound to genomic DNA. Consistent with
 166 our previous findings, Pt-ttpy shows a significant accumulation in cancer cells (11 and 3 times more
 167 than cisplatin and Pt-tpy, respectively) with a slightly higher binding to DNA (1.5 times) (28). Notably,
 168 within mitochondria, Pt-ttpy exhibited stronger accumulation than both cisplatin and Pt-tpy (19 and
 169 8 times more, respectively, as shown in Fig. 1a), It suggests that Pt-ttpy may induce more
 170 dysfunction of mitochondria, as compared with the two other Pt complexes. Next, we studied the
 171 three complexes' effects on mitochondrial genome function including mt DNA copy number
 172 reduction, mt DNA deletion, mt DNA lesion by a real time quantitative PCR method (30) (Fig.1b and

173 c, Supplementary Fig.1), inhibition of mt RNA transcription (Fig.1d) and reduction of the protein
174 levels of mt OXPHOS complexes (Fig.1e and Supplementary Fig.2) in A2780 cells. The induction
175 of mitochondrial genome dysfunction was also detected in another two cancer cell lines Cal27 (Oral
176 squamous cell carcinoma) and H2170 (Lung squamous cell carcinoma) indicated by
177 Supplementary Fig.3. Collectively, these results revealed that Pt-ttpty, due to its higher cellular
178 accumulation and likely to its G4-binding property, shows a high tendency for accumulating in
179 mitochondria with a strong disruption to mitochondrial functions from mt gene replication to its
180 associated protein expression.

181 **Pt-ttpty induces a potent mt dysfunction, but without ROS induction.**

182 To study the consequence of high accumulation of Pt-ttpty in mt with a strong toxicity to mitochondria
183 genome function, we analyzed Pt-ttpty effects on mt function. Interestingly, by FACS and
184 immunofluorescence staining, using TOMM20 antibody (an inner membrane protein of mt), we saw
185 that Pt-ttpty did not induce a significant reduction of the number of mitochondria (Fig. 2a) but a clear
186 mt dysfunctional morphology switch that is also detected in the treatment of cisplatin, but not with
187 Pt-tpy (Fig. 2b). The dysfunctional morphology of mt is consistent with the data collected by real-
188 time mt function monitoring using a Seahorse system (Agilent). mt basal respiration, ATP
189 production as well as spare respiratory capacity were recorded in the presence or absence of the
190 complexes (Fig. 3a). We detected that Pt-ttpty but not Pt-tpy, induced a significant change in cellular
191 respiration (oxygen consumption rate, ATP synthesis and spare respiratory capacity), which
192 suggests mitochondrial dysfunction as one of the modes of Pt-ttpty's action leading to cancer cell
193 proliferation inhibition. We confirmed that cisplatin disrupts mitochondria respiration (31), but in a
194 less pronounced manner than for Pt-ttpty, in correlation with Mitochondrial genome function
195 impairment. Next, we studied the mitochondrial membrane potential by flow cytometry, one of the
196 hallmarks of mitochondrial damage. The change of mitochondrial membrane potential ($\Delta\psi_m$) was
197 detected by JC-1, a well-known probe that accumulates into the mitochondrial membrane matrix
198 space in a manner inversely proportional to $\Delta\psi_m$ (32, 33). Notably, only Pt-ttpty induced a dose-
199 dependent reduction of mt membrane potential (Fig. 3b and Supplementary Fig. 4, which is well
200 correlated to its unique and strong reduction of protein levels of mt OXPHOS complexes, including
201 complexes I, II, III and IV (Fig. 1e and Supplementary Fig. 2). Indeed, there is a strong link between
202 OXPHOS complexes and mitochondrial membrane potential ($\Delta\psi_m$), particularly complexes I, III,
203 and IV are intimately involved in establishing and maintaining $\Delta\psi_m$ (34). Additionally, the loss of $\Delta\psi_m$
204 is reported to be as early event in the process of apoptosis (35), and consistently we detected that
205 Pt-ttpty induced relative more early apoptosis signal by the staining of (Annexin V+/7-AAD-) signals
206 (Supplementary Fig. 5).

207

208 Since ROS (Reactive oxygen species) can induce and/or result from mitochondrial dysfunction
209 (36), total cell and mitochondrial ROS (mt ROS) production was quantified by flow cytometry (Fig.
210 3c and Supplementary Fig. 6 and 7). Consistently with previous works showing that cisplatin's
211 toxicity on mt relies in part on ROS production that dictates cancer cell fate (37), our present data
212 indicates that cisplatin induces both general and mt ROS production for both 24 hours and 96 hours
213 treatments (Fig. 3c and Supplementary Fig. 6 and 7. As well, a slight induction of general ROS was
214 observed after Pt-tpy treatment (Fig. 3c). In contrast, Pt-ttpty did not generate any ROS irrespective
215 of the time of treatments and drug concentration (Fig. 3c and Supplementary Fig. 6 and 7). To
216 further study the unique anti-tumor effects of Pt-ttpty distinct from cisplatin in terms of ROS
217 induction, we conducted a screening of Pt-ttpty and cisplatin effects on another four different tumor

218 cell lines (Hela, H520, H2170 and SK-MES-1) and two primary cells (endothelial cells and fibroblast
219 cells). Indeed, the significant induction of ROS in all tumor cells was only observed in the treatment
220 of cisplatin (Fig. 4). Notably for primary cells, we detected also only cisplatin induced a robust
221 production of ROS in the primary lung tissue fibroblast cells, indicating its potential more side effects
222 to normal tissue, as compared with Pt-ttpy. Collectively, in contrast to cisplatin and Pt-tpy, Pt-ttpy
223 disturbs strongly Mitochondrial genome with a significant induction of mt dysfunction indicated by
224 a high reduction of mt membrane potential, oxygen consumption rate and ATP synthesis, and more
225 early apoptotic signals as well as mt morphology switching, but independent of both general and
226 mt-ROS production that is usually involved in platinum-related cell death induction.

227

228 **Pt-ttpy specifically impairs G4 high enriched nuclear-encoded mt ribosome genes'** 229 **transcription initiation and elongation.**

230 Because we detected that only Pt-ttpy broadly inhibited the protein levels of mt OXPHOS
231 complexes including mt gene-encoded protein CIV-MTCO1 and nuclear gene-encoded protein CIII-
232 UQCRC2/ CIII-Core protein2, CII-SDHB/ CII-30kDa and CI-NDUFB8 (Fig. 1e and Supplementary
233 Fig. 2), but not CV-ATP5A, we hypothesized that Pt-ttpy may also induce mt dysfunction through
234 indirect effects on nuclear-encoded mt related genes. We therefore performed RNA-seq to study
235 the specific impact of Pt-ttpy effects on nuclear-encoded mt associated genes' expression (Fig. 5).
236 To delineate the distinct property of Pt-ttpy in inducing mt dysfunction through mechanisms
237 independent of ROS, we also introduced the setting group of cisplatin for RNA seq (Fig. 5a)). At
238 least, the cisplatin-treated group can serve as a valuable reference for understanding cell death
239 induction mechanisms associated but not restricted to ROS production, thereby possibly
240 distinguishing it from the impacts of Pt-ttpy treatment. Consequently, our study was designed to
241 pinpoint gene(s) related to nuclear-encoded mitochondrial proteins that were specifically down-
242 regulated due to Pt-ttpy treatment, and that effects occurs without the induction of ROS. The
243 process of mining the cohort of genes is depicted in the materials and methods section with the
244 pipeline shown in Fig. 5b. We successfully identified Pt-ttpy specifically down-regulated 14 nuclear-
245 encoded mt OXPHOS genes from a total of 106 genes with mitochondrial pathways showing
246 specific down-regulation due to Pt-ttpy treatment (Fig. 5c on the left). Very interestingly, the
247 largest sub-cohort among these 106 genes (comprising 45 genes) is predominantly involved in the
248 mitochondrial central dogma (38), notably impacting the expression of a majority of nuclear-
249 encoded mt ribosome genes (30 genes) (Fig. 5c, 5d and 5e). Additionally, the remaining 15 genes
250 are primarily related with mt-RNA modifications and its related translation factors (Fig. 5c on the
251 right). Interestingly, when comparing various methods (polymerase stop assays, BG4-ChIP seq
252 and the latest CUT&Tag seq) employed for different databases detailing G4 distribution with
253 distribution of the mt ribosome genes down-regulated by Pt-ttpy (5, 6, 39), we found that most of
254 mt ribosome genes show high G4 abundance in their promoter region (Fig. 5f). These findings
255 suggest that Pt-ttpy potentially targets mt ribosome genes that are highly enriched in G4 structures
256 within their promoter regions, distinguishing them as unique targets in comparison to cisplatin.

257 **Pt-ttpy inhibits the recruiting of TAF1 and NELFB to the nuclear-encoded mt ribosome** 258 **genes' promoter and dampens MT ribosome function.**

259 To validate the RNA-seq findings, we conducted RT-qPCR (Fig.6a) and confirmed that Pt-ttpy
260 exerts a broad inhibiting effects on the expression of mt ribosome genes in A2780 cells.

261 To decipher the mechanisms of how Pt-tpty induces the widespread inhibition of nuclear-encoded
262 mt ribosome genes, first, we explored whether Pt-tpty achieves this by inducing DNA damage within
263 and around the G4-rich regions related with mt ribosome genes. To investigate that, we retrieved
264 our previous work ased on γ -H2AX chromatin immunoprecipitation (ChIP-seq) analysis which
265 suggested that Pt-tpty induces DNA damage in G-rich regions in A2780 cells on the genomic level
266 (as reported in our prior work (28)). However, upon close examination, we found no evidence of
267 DNA damage within the sequence of any of the mitochondrial ribosome genes' sequences upon
268 the same treatment with Pt-tpty. Two represented mt ribosome associated genes' results are
269 presented in Supplementary Fig. 8.

270 Next, we questioned if our G4-ligand Pt-tpty might target the G4-enriched promoter region of mt
271 ribosome genes. This could potentially involve inhibiting the binding of transcription factors (TFs)
272 to their promoters, thus regulating their expression broadly down, because recent works reveal that
273 promoter G4s act as a site for the recruitment of key components of the transcriptional machinery
274 (40), and a reciprocal regulation between native G4 dynamics and gene transcription on genome-
275 wide level by a more sensitive G4-CUT&Tag method (39). So we established a CUT&RUN-qPCR
276 assay using general transcription factors' antibodies, and we clearly see Pt-tpty significantly
277 reduced the occupancy of TAF1 (general transcription factor TFIID subunit) and NELFB (Pol II-
278 associated NELF complex member B) at the specific mt ribosome genes *MRPS18C* and *MPV17L2*
279 promoter and its surrounded regions (Fig. 6b), indicating that Pt-tpty targets mt ribosome genes'
280 promoter G4 enriched region and impairs the recruitment of transcription factors to their promoter
281 and its proximal regions.

282 To further study the consequence of Pt-tpty's inhibiting effects of mt ribosome genes expression
283 that would mostly dampen ribosome-mediated translational machine function, we further tested Pt-
284 tpty effects on mitochondrial specific translation by Click-chemistry-based immunofluorescence (IF)
285 assay with single cell quantification (41), the principle for labeling is presented in Fig.6c left. Clearly,
286 we detected that Pt-tpty show a strong inhibition of mitochondrial translation in A2780 cells (Fig.
287 6c), which is confirmed by another typical cancer cells Hela (Supplementary Fig. S9). Collectively,
288 these data indicate that Pt-tpty impairs the recruitment of transcription initiation and elongation
289 factors of NELFB and TAF1 in nuclear-encoded mt ribosome genes' G4 rich promoter region and
290 inhibits their expression broadly with a significant dampening of mt ribosome function.

291 **Pt-tpty shows significant anti-tumor effects and presents mitochondrial toxicity *in vivo* with** 292 **less side effects, as compared with cisplatin.**

293 To further investigate the potential *in vivo* anti-tumor effects of Pt-tpty, specifically focusing on its
294 impact on mitochondria, we conducted a study using the A2780 xenograft mouse model to assess
295 the effects of Pt-tpty and cisplatin.

296 Based on use of cisplatin for *in vivo* xenografts (intraperitoneal injections at 2 mg/kg) (42), and that
297 Pt-tpty didn't show any *in vivo* toxicities at 5 mg/kg we suggested the intraperitoneal drug
298 administration for Pt-tpty (5 mg/kg) and cisplatin (2 mg/kg), with treatments administered once
299 every two days over a 21-day period. Our findings revealed that Pt-tpty exhibited significant anti-
300 tumor effects with reduced toxicity to normal tissues, particularly the kidney and liver, when
301 compared to cisplatin (refer to Fig. 7a and Supplementary Fig. 10 and 11). Cisplatin is renowned
302 for its capacity to induce nephrotoxicity, a condition that significantly compromises kidney function
303 and is closely linked to intracellular stress responses, prominently oxidative stress (43). We

304 confirmed that cisplatin leads to a decline in liver function, as evidenced by a decrease in the liver
305 index (Supplementary Fig. 10b). Additionally, proximal renal tubular epithelial cells after treatment
306 with cisplatin exhibited turbidity staining and swelling, whereas these effects were less pronounced
307 after treatment with Pt-ttpty (Supplementary Fig. 10c). Concerning the potential liver toxicity caused
308 by all the Pt complexes, cisplatin induced significant inflammation around the portal vein and blood
309 vessels, resulting in enlarged sinusoidal spaces and vascular congestion, effects that were either
310 less prominent or absent in the Pt-ttpty treated group (Supplementary Fig. 11). In terms of potential
311 cardiac toxicity, neither Pt-ttpty nor cisplatin exhibited signs of vascular congestion, fatty
312 degeneration of cardiomyocytes, structural abnormalities, or obvious myocardial rupture
313 phenomena (data not shown). In summary, our studies indicate that Pt-ttpty offers a relatively safer
314 profile compared to cisplatin.

315 Through RT-qPCR analysis on tumor tissue samples, consistent with our *in vitro* study, only Pt-ttpty
316 showed significant inhibition of nuclear-encoded mt ribosome genes (Fig. 7b) and mt-encoded
317 genes (Fig. 7c) and protein expression levels (Fig. 7d and e). In contrast with our prior *in vitro* study,
318 Pt-ttpty did not show clear effects on mt DNA copy number in the *in vivo* tumor samples (Fig. 7f),
319 which would be explained by the high variation of mt DNA copies in tumor tissues (44). Collectively,
320 we proposed a model of Pt-ttpty-mediated profound inhibition on mitochondrial genome in cancer
321 cells through a direct effect on mitochondria and an indirect effect based on broad inhibition of G4-
322 enriched nuclear-encoded mt ribosome genes expression.

323 **Discussion**

324 Given the evidence that mitochondria can be the targets of G4-interactive compounds (9) (10) and
325 platinum complexes (31, 45-47), we envisioned that Pt-ttpty that combines G4-binding properties
326 and a platinum coordinating moiety, may localize in mitochondria and play a significant role in the
327 mechanisms underlying mitochondrial toxicity. In this line, we raised the questions about whether
328 and how this small molecule affects the processes associated with mitochondrial function based
329 on its unique dual properties. To this aim, we performed a comprehensive *in vitro* and *in vivo*
330 mechanistic study of Pt-ttpty on both nuclear and mt genome in regulating mt homeostasis and thus
331 explore its potential anti-cancer therapeutic benefits, comparing with two other Pt complexes: a
332 close structural analogue, Pt-tpy that display a weak/non G4-binding property and the prevalent
333 and well-established chemotherapy agent cisplatin. We demonstrated that Pt-ttpty shows a strong
334 disturbance to mitochondrial genome and its function, both *in vitro* and *in vivo*. Mechanistic studies
335 suggest Pt-tpy's potent dysfunction of mitochondria is related to its direct targeting to mitochondria
336 *via* its high accumulation in mitochondria and indirect targeting to mitochondria through inhibiting
337 mt ribosome associated genes' expression in chromatin by impairing the recruitment of TF to their
338 G4 rich promoter and proximal regions. Notably, the global impact of Pt-ttpty on mitochondria does
339 not induce ROS production that is, otherwise, typically contributing to platinum complexes
340 treatment-related side effects. Importantly, these data are correlated with *in vivo* evidence of Pt-
341 ttpty presenting more reduced side effects with effective anti-cancer benefits, as compared with
342 cisplatin.

343 Increasing evidence supports the ability of mitochondrial DNA (mt DNA) to form G4 in cancer cells,
344 and mt G4 dysregulation affects mt nucleic acid synthesis (13) and mt function as well as mt DNA
345 deletion formation (21). Interestingly using our G4 ligand Pt-ttpty, we detected its high accumulation
346 in mitochondria with a strong disturbance to mitochondrial genome in cancer cells A2780, whereas
347 its counterpart Pt-tpy with low/no G4 binding property is almost inactive. Pt-ttpty induced mt DNA
348 deletion, interfered with mt replication, transcription, and protein synthesis, leading to mitochondrial

349 dysfunction indicated by mitochondrial membrane potential modification, ATP levels decrease, and
350 markers of mitochondrial damage including a toxic mt morphology switching. Interestingly as
351 compared to another G4 specific ligand RHPS4 used in non-cancerous cells (21), Pt-tpty does also
352 present direct targeting of mitochondria. Indeed both compounds RHPS4 and Pt-tpty are lipophilic
353 cations which makes them good candidates for being trapped in mitochondria through strong
354 electrostatic attraction due to the highly negative membrane potential of the inner mitochondrial
355 membrane as is well known (29). This phenomenon should constitute a first step contributing in
356 part and in a non-specific manner, to the high accumulation of Pt-tpty (and RHPS4) in mitochondria.
357 Secondly, we suspected that Pt-tpty, like RHPS4, may directly target mt DNA *via* stabilization of
358 some G4s, since neither Pt-tpty, nor cisplatin, two non-or low- G4 binders, induced a strong effect.
359 Furthermore, we detected a more potent mt DNA lesion for Pt-tpty that can be attributed to the
360 direct binding of Pt-tpty to mt DNA through metallic coordination to nucleic bases (24). Indeed, we
361 can exclude that the mt lesion is due to oxidized guanine (30) since Pt-tpty does not produce ROS,
362 in contrast to cisplatin (37). Nevertheless, unlike RHPS4, which appeared to modulate varying
363 levels of mt gene expression, possibly through interactions with the predicted G4 structures in H-
364 stand DNA template in non-cancer cell model (21), Pt-tpty induces a potent but non-differential
365 inhibition of mitochondrial gene transcription in both the heavy and light strands of mt DNA genes
366 in cancer cells. The disparity may originate, at least, from the fact that epithelial cancer cells exhibit
367 a higher mitochondrial membrane potential ($\Delta\Psi_m$) than their normal counterpart cells (48). In
368 addition, these differences may arise also from a collecting factors: including the specific cell model
369 employed used with different inherent ability to form G4s (39), the ligands' capacity to stabilize mt
370 DNA G4 structures, and the distinct treatment protocols applied. A better knowledge of the above
371 factors holds the potential to guide the rational design of personalized anti-cancer treatment
372 strategies of targeting cancer cells' mt DNA G4.

373 Importantly, apart from Pt-tpty direct impact on mitochondria, likely through a G4-dependent
374 mechanism, which triggers a cascade of disruptions in the mitochondrial genome, Pt-tpty also
375 targets G4 structures in the nuclear genome. It has the potential to influence mitochondrial
376 homeostasis (1). More specifically, the modulation of G4-rich chromatin regions may conceivably
377 lead to mitochondrial dysfunction. Indeed, nearly around 99% mitochondrial functional proteins are
378 not encoded in mt genome but in nucleus. Notably in this study, we detected that only Pt-tpty
379 decreased all mt OXPHOS complexes' protein expression, including CI subunit NDUF8, CII-
380 30kDa, CIII-Core protein2 and CIV subunit1, except for CV alpha subunit. Since the proteins down-
381 regulated by Pt-tpty treatment are not restricted to mitochondrial genome-encoded MTCO1 (CIV
382 subunit1), these data lead us to define alternative G4 forming sequences, beyond mt genome, to
383 decipher the underlying mechanism behind Pt-tpty strong disturbance to mitochondrial function
384 without ROS production, especially as compared with the ROS-related mt toxicity-inducing
385 molecule i.e cisplatin. Through RNA-seq and Cut&RUN assay using transcription factors'
386 antibodies, different G4 distribution databases, our work indicates firstly that the promoter region
387 of most mitochondrial ribosomal genes are highly enriched in potential G4 forming sequences, in
388 correlation with the previous finding that G4s in 5'UTR of mRNA coding for ribosomal protein can
389 control their production (49). Moreover Pt-tpty, by stabilizing G4, would impair the recruitment of
390 transcription factors to the mt ribosome genes' G4 forming sequences-related chromatin and
391 decrease mt ribosome genes expression with a functional impairment of mitochondrial ribosome-
392 involved translation process. This work revealed, for the first time on genomic DNA level, that the
393 genes for human mitochondrial ribosomal proteins (MRPs) are targets of the G4 ligand Pt-tpty.
394 Since increasing data suggested the potential of Mitochondrial Ribosomal Genes as Cancer

395 Biomarkers (50, 51), further investigation is warranted to develop and elucidate the promising anti-
396 cancer effects of the G4 ligand i.e Pt-tpty, particularly when targeting selectively overexpressed
397 MRPs in special cancer types.

398 In terms of mitochondrial dysfunction, cisplatin has been shown to have significant effects on that
399 (37) (52, 53). One of the mechanisms underlying cisplatin-induced mitochondrial toxicity is the
400 generation of ROS, leading to oxidative stress-induced cell death, which is also a well-defined
401 source of cisplatin-induced side effects (54) (55, 56). In this regard and notably, Pt-tpty does not
402 function like typical Pt complexes, likely for cisplatin and Pt-tpy, as it neither induces general ROS
403 nor mt specific ROS production in both cancer cell lines and primary tissue cells for short and long
404 time (Fig.3c, 4 and Supplementary Fig. 6 and 7). This inspiring property of Pt-tpty-induced mt
405 dysfunction independent of ROS production might be directly correlated with lower toxicity to liver
406 and kidney observed through *in vivo* studies when compared with cisplatin. Continuing to
407 investigate whether other G4 ligands exhibit similarly to Pt-tpty-induced mitochondrial dysfunction
408 independent of ROS production, could provide valuable insights into the role of oxidative stress-
409 independent mitochondrial toxicity. This knowledge is also beneficial for the development of
410 platinum-based compounds with enhanced safety profiles.

411 In summary, we showed that Pt-tpty, a G4-binding platinum complex, disrupts significantly
412 mitochondrial function both *in vitro* and *in vivo*. Overall, Pt-tpty shows a direct and high
413 accumulation in mitochondria with a potent inhibition of mitochondrial genome function and
414 dampens mt homeostasis in the absence of oxidative stress, which distinguishes it from the
415 conventional platinum-derived clinical drug cisplatin that primarily exerts toxicity on mitochondria
416 through ROS induction. Moreover, Pt-tpty hinders the recruitment of transcription factors to the G4-
417 prone promoter regions of most nuclear-encoded mitochondrial ribosome genes, thereby leading
418 to a broad reduction in the expression of these genes and impairing the functional efficiency of
419 mitochondrial ribosome-involved translation processes. Hence, the *in vitro* and *in vivo* studies of
420 Pt-tpty's activity conducted herein provided us with valuable insights into the therapeutic prospects
421 of drugs targeting mitochondria without generating ROS. Importantly, our work holds strong
422 promise of developing G4-binding platinum-based compounds with improved safety profiles
423 alongside effective anti-cancer benefits.

424

425 **Materials and Methods**

426

426 **Cell culture**

427 Ovarian cancer cell line A2780 (catalog no. CTCC-003-0011, Meisen CTCC), Cervical cancer cell
428 line Hela (catalog no. CTCC-001-0006, Meisen CTCC), non-small cell lung cancer (NCLC) cell line
429 H2170 (catalog no. CTCC-400-0050, Meisen CTCC) and Mouse primary Lung micro-endothelial
430 cells were purchased from Zhejiang Meisen Cell Technology Co., Ltd. Oral squamous cell carcinoma
431 cell line Cal27 is a kind gift from the lab of Prof. Qin He from West China school of Pharmacy, and
432 NCLC cell lines H520 and SK-MES-1 are kind gifts from the lab of Prof. Zhoufeng Wang from West
433 China hospital. Human primary lung fibroblast cells were sorted by CD106 antibody (#130-122-
434 339, Miltenyi Biotec) with the kit of Dynabeads™ FlowComp™ Flexi (#11061D, ThermoFisher).
435 Human cancer cells A2780, H2170, H520 and human primary fibroblast cells were cultured in
436 complete RPMI 1640 medium supplemented with 10% fetal bovine serum (FBS, catalog no.
437 Z7185FBS-500, ZETA life) and 100 U/ml penicillin + 100 ug/ml streptomycin (catalog no. Gibco-
438 15140122, ThermoFisher, Gibco). Cancer cells Hela, and Cal27 were cultured with DMEM medium
439 with 10%FBS with penicillin and streptomycin. Cancer cells SK-MES-1 were cultured with MEM- α

440 medium with 10%FBS with penicillin and streptomycin. Primary mouse lung micro-endothelial cells
441 were cultured with Lonza EGM-2 MV microvascular endothelial cells growth medium-2 Bulletkit
442 (#CC-3202). Cells were incubated under a 5% CO₂ humidified incubator at 37°C. When it reached
443 80%-90% fusion, cells were digested with 0.25% trypsin/0.91 mM EDTA (catalog no. Gibco
444 2520072, ThermoFisher), then collected for indicated experiments.

445 **Platinum complexes**

446 Cisplatin (CisPt) was provided from MCE. MedChemExpress (catalog no. HY-17394). Pt-tpty
447 (tolylterpyridine platinum complex) and Pt-tpy (terpyridine platinum complex) were synthesized
448 following the procedure already described (23) (Scheme 1). Pt-tpty was also provided from Merck
449 Sigma (catalog no. SML2556). Aqueous solutions of 1 mM cisplatin, of 1 mM Pt-tpy, and 6 mM
450 DMSO (catalog no. D2650 10 ml, Merck, Sigma Aldrich) solutions of Pt-tpty were prepared and
451 conserved at -20°C. Diluted solutions of each molecule were freshly prepared. The drugs were
452 used at their iso-effect concentrations that inhibit 80% (IC₈₀ concentrations) cell proliferation after
453 96 h that are 0.6 μM, 5.5 μM and 7.5 μM, for cisplatin, Pt-tpty and Pt-tpy, respectively, unless
454 indicated otherwise.

455 **Platinum measurement**

456 The platinum cellular uptake was quantified by ICP-MS (Inductively Coupled Plasma Mass
457 Spectrometry, NexION® 2000, Perkin Elmer, Courtaboeuf, France) on cellular pellets (5 × 10⁶ cells),
458 DNA extracts as previously described (28), and on isolated mitochondria. A2780 cells were treated
459 with the IC₈₀ concentration of cisplatin, Pt-tppy and Pt-tpy for 96 hours. DNA (quantified by
460 nanodrop) was extracted from cell pellets using the DNeasy Blood & Tissue Kit (Qiagen) and
461 mitochondria were isolated using the Mitochondria Isolation Kit for Cultured cell pellets (2 × 10⁷
462 cells) (Thermo Scientific). Prior to ICP-MS, the samples were digested with pure nitric acid
463 (PlasmaPURE® Plus HNO₃ 67-69%, SCP Science, Courtaboeuf, France) at 95°C for cell pellets,
464 and HNO₃ 0.1 M for DNA and mitochondria. The Pt content was determined following a dose
465 response curve established from known concentrations of platinum. The amount of platinum was
466 then reported as ng of Pt/5 × 10⁶ cells for pellets, pg Pt/μg DNA or ng of Pt/5 × 10⁶ cells for
467 mitochondria.

468 **Measurement of mitochondrial respiration**

469 A2780 cells were seeded in a Seahorse XF96 96-well cell culture plate (Agilent) (8,000 cells/well,
470 80 μL of RPMI medium completed with 10% FBS and penicillin/streptomycin). The plate was
471 incubated for 1 h at r.t. and then at 37 °C, 5% CO₂ overnight. Cells were then treated with
472 compounds dilutions (10 μM) and incubated for an additional 24 hours at 37 °C, 5% CO₂. The
473 seahorse Mitostress test was then performed in accordance with the manufacturer instructions
474 using inhibitors solution at the following final concentrations: [oligomycin] = 1.5 μM, [FCCP] = 0.5
475 μM, [Rotenone] = [Antimycin A] = 0.5 μM. Following the assay, the medium was carefully removed,
476 and cells were fixed with 100 μL of 4% PFA in PBS for 10 min at room temperature. Cells were
477 then washed twice with PBS and incubated with 100 μL of ca. 3 μM Hoechst 33342 (NucBlue™)
478 for 10 min at r.t. Cells were washed twice with PBS and directly imaged with a Cytation 5 (Agilent)
479 using a 4X objective focused on the center of the well and a DAPI imaging cube. Raw assay data
480 were normalized using the cell coverage in each well image using the Gen5 software.

481 **Total ROS or Mitochondrial ROS detection by FACS**

482 For total ROS production detection, A2780 cells are cultured with the initial concentration of 0.2×10^5
483 cells/ml in a 6 well plate at their IC_{80} concentration (or 10 μ M). After 96 hours (or 24 hours)
484 treatment, CellROX Deep Red (Molecular Probes) was added at the final concentration of 500-
485 1000nM to the cells and incubated at 37°C. After washing with PBS, analyze was performed using
486 the flow cytometry and detection at 635 nm excitation for the CellROX Deep Red reagent
487 (Invitrogen).

488 For Mitochondria ROS detection, it is based on the modified protocol from MitoSOX (M36008,
489 Invitrogen)-based FACS method (57). Cells are cultured with the initial concentration of 0.5×10^6
490 cells/ml in a 6 well plate with the complexes Pt-tpy, Pt-tpy and cisplatin at the concentration of 10
491 μ M. After 24 hours treatment, cells were washed with pre-warm PBS in 6-well plate for 1 time. After,
492 1 μ M Mito-sox was added in each well and incubated for 30 min at 37°C. Wash cells thoroughly
493 with pre-warm PBS for another 3 times, followed by trypsin and cells collection. Using loading buffer
494 (2% FBS in PBS) to collect and mix well cells (working volume is 500 μ l) and move to BD
495 FACSCanto studies.

496 **Total ROS and mitochondrial specific ROS simultaneously detection by high content** 497 **microscope screening followed by single cell quantification**

498 Investigating simultaneously the total ROS (ROS Assay Kit-Highly sensitive DCFH-DA, #R252,
499 DOJINDO) and Mitochondria ROS (mtSOX Deep Red-Mitochondrial Superoxide dection #MT14,
500 DOJINDO) induction post Pt-tpy or cisplatin treatments was performed following manufacturer's
501 protocol. Briefly, indicated cells were treated with cisplatin and Pt-tpy for 1 day at the con. of 10
502 μ M for cancer cell lines or 1 μ M for primary cells. After, the living cells was incubated simultaneously
503 with different dye for 30min at 37°C. Then, the images were collected with ECLIPSE Ni-E (Nikon)
504 microscope with highly sensitive camera, FITC channel for the detection of total ROS (ex: 488nm),
505 Red channel for the detection of mt-ROS (ex:621nm). Single cell fluorescence intensity was
506 unbiased quantified by Image J using in-house developed Macros, at least 50 cells were quantified
507 for each group. And the quantification results were statistically analyzed using GraphPad Prism
508 9.0.

509 **Fluorescent quantitative PCR and fluorescent quantitative RT-PCR**

510 SYBR probes (POWRUP SYBR MASTER MIX, catalog no. A25742, applied biosystems by Thermo
511 Fisher Scientific) were used in a 25ul system. Reaction conditions were following the manufacturer's
512 protocol.

513 For *in vitro* samples, total RNA from A2780 cells untreated and treated by the various platinum
514 complexes at their IC_{80} concentrations for 96 hours was extracted using the RNA simple Total RNA
515 kit (catalogue no. DP419, TIANGEN), and then taken 1 μ g after quantification for reverse
516 transcription. After removal of residual DNA using DNase I, RNase-free (catalogue no. EN0529,
517 thermo scientific), RevertAid MM (catalogue no.M1631, thermo scientific) was added and reversed
518 to cDNA using a PCR instrument (Bio-Red).

519 For *in vivo* samples, tumor tissue DNA was extracted using the FastPure®DNA Isolation Mini Kit
520 (catalogue no. DC112-02, Vazyme) and diluted to 10 ng/ml. Total tumor tissue RNA was extracted
521 using the FastPure®Total RNA Isolation Mini Kit (catalogue no.RC112-01, Vazyme) and
522 subsequently reverse transcription was performed as before. Real-time qPCR was carried out

523 using a QuantStudio 3 Real-Time qPCR System (Applied Biosystems). The primers used are
524 shown in the Supplementary Table 1.

525 **qPCR-based method for quantification of mtDNA copy numbers including deleted and non-** 526 **deleted isoforms.**

527 Investigating the relative changes of mtDNA copy numbers is based on qPCR method. Total DNA
528 for indicated *in vitro* cell samples untreated and treated by the various platinum complexes at their
529 IC₈₀ concentrations for 96 hours or *in vivo* tumor samples were extracted using DNA Blood and
530 Tissue Kit (Qiagen, Germany). DNA quantity was determined by NanoDrop (Thermo Fisher). The
531 DNA showed a high purity (A260/ A280>1.8) and was stored at -20°C. The primers used for real
532 time amplification were synthesized and HPLC-purified by Eurogentec. Because the most common
533 aberrancy is a 4,977-bp deletion spanning nucleotides 8,483–13,459 of the mitochondrial genome
534 (58), different primers were used for detecting mtDNA deleted (also known as mtDNA⁴⁹⁷⁷) and non-
535 deleted isoforms, as well as total mtDNA including both isoforms. Their primers' location are
536 indicated in Figure. 1b. The primers of 12S, tRNA are used for quantification of total mtDNA, and
537 the primers of ND4 and COX III are used for quantification of non-deleted mtDNA. All the above
538 primers are listed in the Supplementary Table 1. The primers used for deleted mtDNA isoform
539 (mtDNA⁴⁹⁷⁷) quantification is covering the gene ND5 and ATPase8, and common deletion primer
540 Forward: TTCCTCATCACCCAATAAAAA, common deletion primer Reverse:
541 TTCGATGATGTGGTCTTTGG. Real-time qPCR was carried out using a QuantStudio 5 real-time
542 PCR system by conventional settings (Applied Biosystems).

543 **RNA sequence**

544 A2780 cells were plated in 10 cm dishes and divided into three groups: UT, Pt-tpty and cisplatin.
545 The cell seed densities for each group were as follows: 0.5 X 10⁶ cells per dish for UT, 1.5 X 10⁶
546 and 1.5 X 10⁶ cells per dish for both Pt-tpty and cisplatin. After a two-hours incubation, the
547 corresponding drugs were added to each group at their IC₈₀ concentration for 96-hours treatment
548 period. At the end of the incubation period, the cells were washed twice with Hank's Balanced Salt
549 Solution (HBSS, catalog no. C14175500BT, ThermoFisher, Gibco), subsequently, they were
550 treated with the cell lysis solution TRIzol (catalogue no. 15596026, ThermoFisher, invitrogen) at
551 room temperature for 5 min. Afterward, the cells were gently scraped off with a cell scraper and
552 collected in centrifuge tubes, remained at room temperature for an additional 5 min. Finally, the cell
553 samples were snap-frozen in liquid nitrogen and stored in an ultra-low temperature refrigerator,
554 which would be used for RNA extraction just before conducting RNA sequence. Three distinct and
555 independent samples were collected for each group.

556 RNA transcriptomics sequencing was conducted by Biomarker Technologies on each set of three
557 parallel samples. After successfully passing the library quality check, pooling was performed
558 according to the target downstream data volume and sequencing was carried out using the Illumina
559 platform. Clean data was filtered for sequence alignment with the reference human genome, and
560 mapped data was obtained for library quality assessment such as insert length testing and
561 randomness testing. Structural-level analysis such as variable splicing analysis, novel gene
562 discovery and gene structure optimization were also performed. Differential gene expression
563 analysis was conducted to identify differences in gene expression among different samples or
564 sample groups. The data was graphically by R for MacOSX to generate the figures included in the
565 manuscript.

566 To identify genes related to nuclear-encoded mitochondrial proteins that were down-regulated
567 specifically by Pt-tpty treatment, we firstly identified the genes exhibiting down-regulation in the Pt-
568 tpty group as compared to the UT group (with criteria FDR < 0.05, FC > 1.2). These genes were
569 then intersected with the gene list of nuclear-encoded mitochondrial proteins (38). A parallel
570 analysis was performed for the cisplatin group. Subsequently, the two resulting gene lists were
571 intersected to identify the cohort of genes specifically down-regulated in the Pt-tpty group, not in
572 the cisplatin group.

573 **CUT&RUN-qPCR**

574 Experimental reagents were used with Vazyme's Hyperactive pG-MNase CUT&RUN Assay Kit for
575 PCR/qPCR (catalogue no. HD101, Vazyme). A2780 cells were plated in 10 cm dishes in DMSO
576 and Pt-tpty groups at a cell density of 1×10^6 and 3×10^6 . After two hours of seeding, Pt-tpty at IC_{80}
577 concentration was added in indicated dishes. And a corresponding volume of DMSO (<1%) was
578 added to the DMSO group as control and incubated at 37°C for 96 hours. Cells were collected by
579 trypsin digestion and dispensed into 0.5×10^6 /tubes. Subsequent steps were performed according
580 to the experimental protocol (59). Specific antibodies are used to bind to transcription complexes
581 and pull-down specific fragments of DNA sequences by enzymatic cleavage and purification: TAF1
582 (TAF1 Rabbit mAb catalogue no.#12781S, D6J8B, CST) and NELFB (COBRA1 Rabbit mAb
583 catalogue no.#14894S, D6K9A, CST) antibodies. After quantification of the pulled-down DNA
584 sequences, primers, and probe SYBR were added for qPCR. Five pairs of primers were designed
585 in the 1.5 Kb region around the TSS of the *MPV17L2* and *MRPS18C* genes to examine the
586 distribution of different transcription factors and the effect of the drug Pt-tpty on them. The samples
587 subjected to qPCR expression analysis using SYBR Green probe by PowerUp SYBR Green Master
588 Mix (catalog no. A25742, Applied Biosystems from Thermo Fisher Scientific). The PCR
589 amplification was performed on QuantStudio 3 Real-Time PCR System (Applied Biosystems) with
590 the conventional setting parameters, 40 cycles at 95 °C for 15 s, 60 °C for 1 min. The Mean
591 threshold cycles were determined from three technical repeats using the comparative CT
592 methodology. To standardize expression levels, they were normalized to that of actin.

593 **Click-chemistry for IF study of MT translation with single cell quantification**

594 A2780 or Hela cells were inoculated on 14 mm coverslips (catalogue no.WHB-24-cs, WHB) in 24-
595 well plates, walled for 4 hours and then treated with the Pt-tpty (IC_{80} : 5.5 μ M) and corresponding
596 DMSO for 96 hours. The medium was gently refreshed by L-Methionine-free 1640 medium
597 (catalogue no.CTCC-002-148, Meisen CTCC) and each well was treated with 100 ug/ml
598 Cycloheximide (CHI, catalogue no.HY-12320, MedChemExpress) and incubated for 30 min at 37°C
599 to stop protein translation in the cytoplasm ; In addition to this positive control, 80ug/ml of
600 Chloramphenicol (catalogue no.HY-B0239, MedChemExpress) was added and incubated for 30
601 minutes at 37°C to stop mitochondrial protein translation; 500 μ M of methionine analogue-
602 homoacetylglycine HPG (catalogue no.HY-140345A, MedChemExpress) was added to each well
603 and incubated for 60 min at 37°C to insert it into the nascent protein peptide chain. Before fixation,
604 cells were permeabilized in pre-chilled buffer A (10 mM HEPES; 10 mM NaCl; 5 mM MgCl₂ ; 300
605 mM sucrose) containing 0.015% digitonin (catalogue no.HY-N4000, MedChemExpress) for two
606 minutes, followed by 15 s reaction in buffer A without digitonin; 4% PFA (catalogue
607 no.BL539A, Biosharp) fixed cells for 10 min, washed that in PBS and permeabilized that in 0.1%
608 Triton X-100 (catalogue no.9002-93-1, Solarbio) for 20 min; 3% BSA (catalogue no.9048-46-8,
609 Merck Sigma) was used for blocking for another 30 min and the cells were treated with 20 μ M of

610 Alexa Fluor® 488 (labeled to azide , catalogue no.A10266, ThermoFisher, Invitrogen) that had
611 been diluted to the antibody reaction solution (100 mM Tris, 100 mM ascorbic acid, 1 mM CuSO₄)
612 for the click reaction in 15 min at room temperature (41); after washing with PBS, 1 µg/ml of DAPI
613 (catalogue no.28718-90-3, MedChemExpress) was added at room temperature for another 5 min.
614 After washing with PBS, slides were sealed to air-dry in hood. Images were collected with ECLIPSE
615 Ni-E (Nikon) microscope using oil with the 40x objective.

616 Single cell fluorescence intensity was unbiased quantified by Image J using in-house developed
617 Macros, at least 200 cells were quantified for each group. And the quantification results were
618 statistically analyzed using GraphPad Prism 9.0.

619 **Immunofluorescence (IF) study of mitochondrial morphology and quantification of** 620 **mitochondria by FACS (TOMM20 labeling)**

621 For IF studies by TOMM20 labeling, A2780 cells were plated firstly on 8-well labteks (Thermo fish
622 scientific). Cells were treated for 96 hours at their respective IC₈₀ concentrations (see main text).
623 After treatment, cells were washed with PBS, then fixed 10 minutes in 2% Paraformaldehyde (PFA).
624 After wash with PBS, cells were permeabilized for 10 min at RT using 0.2% Triton X-100 and
625 washed with PBS. The cells were incubated in blocking buffer (5% goat serum in PBS) for 60 min
626 at RT before being incubated at 4°C overnight in 1% BSA dissolved in PBS with the primary
627 antibody against TOMM20 (Abcam). On the second day, after three times wash with PBS, the cells
628 were incubated for another 30 min with the Alexa Fluor 555-conjugated secondary antibody (Life
629 Technologies). Nuclei were labeled using DAPI and the cover slides were mounted with
630 Vectashield™. Acquisitions were performed on Leica SP5 confocal microscope by the microscopy
631 platform of the Institut Curie.
632

633 For FACS studies by TOMM20 labeling, A2780 cells were plated firstly on 100 mm dishes (Thermo
634 fish scientific). Cells were treated for 96 hours at their respective IC₈₀ concentrations (see main
635 text). After treatment, cells were washed with PBS, followed by trypsin to collect cells. Suspend
636 cells at around 2x10⁶ in 250 µl washing buffer (PBS+0,5%BSA) with another 250 µl 4% PFA. Mix
637 well and fix samples for another 10 min at r.t. After permeabilization with 0.2% Triton X-100, cells
638 were stained with TOMM20 antibody (Abcam) for 15min by gentle rotation at 4°C, followed by 3
639 times thoroughly wash with PBS. After, cells were incubated with 1 µl second antibody-PE in dark
640 for another for another 10 min by gentle rotation at 4°C (working volume is 200 µl). Wash thoroughly
641 cells with 1ml permeabilization buffer for another 2 times, then prepare 400 µl washing buffer to
642 collect and mix well cells and move that for BD FACSCanto studies.

643 **Tumor xenografts studies**

644 SPF-rated BALB/c nude mouse (6 weeks old) weighting 20-22 g were purchased from Chengdu
645 Dossy Laboratory Animal Company. Before the beginning of the experiment, animals were
646 acclimatized in a temperature-controlled environment for 1 week. The nude mice were housed in
647 individually ventilated cages fed a normal diet and water under artificially controlled environment
648 (temperature 20±2°C, humidity 50%-60%, photoperiod: 12 h light, 12 h dark). Murine experiments
649 were carried out following the guidelines of medical research and new medical technology of
650 Sichuan Cancer Hospital Ethics Committee and performed under study number SCCHEC-02-
651 2023-064. All methods were performed in accordance with Guide for the Care and Use of
652 Laboratory Animals.

653 A2780 cells in the exponential growth phase were collected and resuspended in 50 ul of RPMI
654 medium per 1×10^7 cells, and the same volume of cell matrix (catalogue no.356234, Corning®
655 Matrigel® Matrix) was mixed to the cell suspension in ice. Suspended A2780 cells (1×10^7
656 cells/mouse) were injected subcutaneously on the back next to the right leg in a sterile environment
657 on an ultra-clean table. After injection for 5 days, they were randomly divided into 3 groups
658 according to the size of the tumor volume ($V=L^2 \times W \times \pi/6$) equally, namely DMSO, Pt-ttpy and
659 cisplatin t groups. The nude mice in the three groups were injected intraperitoneally with 400 ul of
660 1% DMSO, Pt-ttpy (5 mg/kg) and cisplatin (2 mg/kg) once every two days for 21 days. The body
661 weight and tumor volume of each nude mouse were recorded during this time. When dosing was
662 complete, all nude mice were euthanized and the tumors were isolated, rapidly cooled in liquid
663 nitrogen or stored at ultra-low temperature refrigerator for further studies. Major tissues, including
664 the liver, kidney, and heart, were weighted, the tissue index was calculated as the ratio of tissue
665 weight (g) to body weight (g): tissue index % = liver weight (g) / body weight (g) * 100. Then, a
666 preliminary major tissue toxicity study was performed using typical HE staining.

667 **Western blotting (WB)**

668 For *in vitro* cell pellets samples preparation, $0.2-0.3 \times 10^6$ /well A2780 cells was plated in 6-well
669 plate with full medium for 24 hours, then full medium was removed, and cells were refreshed with
670 indicated treatments with metallic complexes at their IC_{80} concentration for 24 hours or 96 hours.
671 After, total proteins were extracted using RIPA 1X buffer (Cell Signaling Technology, CST)
672 supplemented just before use with 1X EDTA-free Protease Inhibitor Cocktail (Roche), 20 mM NaF
673 and 1 mM Na_3VO_4 . Around 20 μ g proteins were loaded onto Mini-PROTEAN Precast gels
674 (BioRAD) for further WB procedures.

675 For *in vivo* tumor tissue samples preparation for western blotting, proteins were isolated from tumor
676 tissue using a 3-min ultrasonic cycle homogenization (cycle of 15 s sonication, 10 s resting time)
677 in ice, followed by a 30 min more extraction in ice using RIPA (CST) 1X buffer supplemented just
678 before using with protease and phosphate inhibitors (HY-K0022/K0023, MCE®
679 MedChemExpress). Samples were vortexed for 15 s by every 15min. After centrifugation for 20min
680 at 14,000 rpm at 4°C, supernatants were collected, and protein amount was quantified for each
681 group or mice using BCA. The separation of proteins was performed using either Mini-PROTEAN
682 Precast gels (BioRAD) or NuPAGE 4-12% gels (Life Technologies).

683 After, proteins were transferred to PVDF membranes (catalogue no.ISEQ00010, Immobilon ®-
684 PSQ, MERCK Millipore Ltd.) with 90V for 90min by BioRAD wet transfer system or semi-dry transfer
685 method using Trans-Blot Turbo Transfer system (BioRAD) with the settings of 1.3A-25V-7M.
686 Primary antibodies (MTCO1, 1:1000, Abclonal; β -Tubulin, 1:8000, Abclonal; actin, 1:3000, CST;
687 total OXPHOS human WB antibody cocktail, 1:1000, Abcam) were diluted with 5% BSA and
688 incubated overnight at 4°C, then the membranes were incubated with secondary antibodies (HRP
689 Goat Anti- Rabbit IgG(H+L), 1:5000, Abclonal, or HRP-conjugated Affinipure Goat Anti-Mouse
690 IgG(H+L), 1:5000, proteintech) at room temperature for another 2 hours. WB detection was
691 performed by chemiluminescence (BioRAD) with traditional X-ray films (FIJIFILM) or digital CDD
692 imaging (BioRAD or Vilber). The intensity of indicated band was measured by ImageJ (NIH
693 software).

694 **Statistical analysis**

695 The data were analyzed using Graphpad Prism 9.0 software (San Diego, CA). The results were
696 presented as either mean \pm SEM or \pm SD as indicated, details of regarding the number of
697 experimental replicates and statistical analyses methods were indicated in the figure legends.

698 **Acknowledgments**

699 The authors are grateful for the support provided by the public experimental platform from West
700 China School of Pharmacy and Wang Wendong for critical and very useful advice on pathology
701 and toxicology. The authors also greatly acknowledge Cédric Messaoudi, Marie-Noelle Soler and
702 Laetitia Besse from the Multimodal Imaging Center - CNRS UMS2016 / Inserm US43 / Institut Curie
703 / Université Paris-Saclay - for useful advice on image processing and Charlene Lasgi for technical
704 help on flow cytometry (Flowcytometry Orsay facility, Curie). The authors profoundly thank Prof.
705 Yinglan Zhao (State Key Laboratory of Biotherapy) for a long tradition of insightful discussions with
706 excellent comments and suggestions.

707 This research was funded by Science and Technology Department of Sichuan Province
708 2023NSFSC0130 and 2023NSFSC1992, and “the Fundamental Research Funds for the Central
709 Universities”, as well as Institute Curie Grants to TJ. This research was funded also by Centre
710 National de Recherche Scientifique (CNRS), Institut National de la Sante et de la Recherche
711 Medicale (INSERM), Institut Curie, Paris-Saclay University, Association pour la Recherche contre
712 le Cancer (ARC grant for DP). This project has received funding from the European Union’s Horizon
713 2020 research and innovation program under the Marie Skłodowska-Curie grant agreement No
714 666 003 (Grant for DP). This work was also financially supported by an ERC Consolidator Grant
715 Photo-MedMet to G. G. (GA 681679), has received support under the program “Investissements
716 d’Avenir” launched by the French Government and implemented by the ANR with the reference
717 ANR-10-IDEX-0001-02 PSL (G. G.) and by a Qlife prématuration funding (G.G. and R.V.).

718 **References**

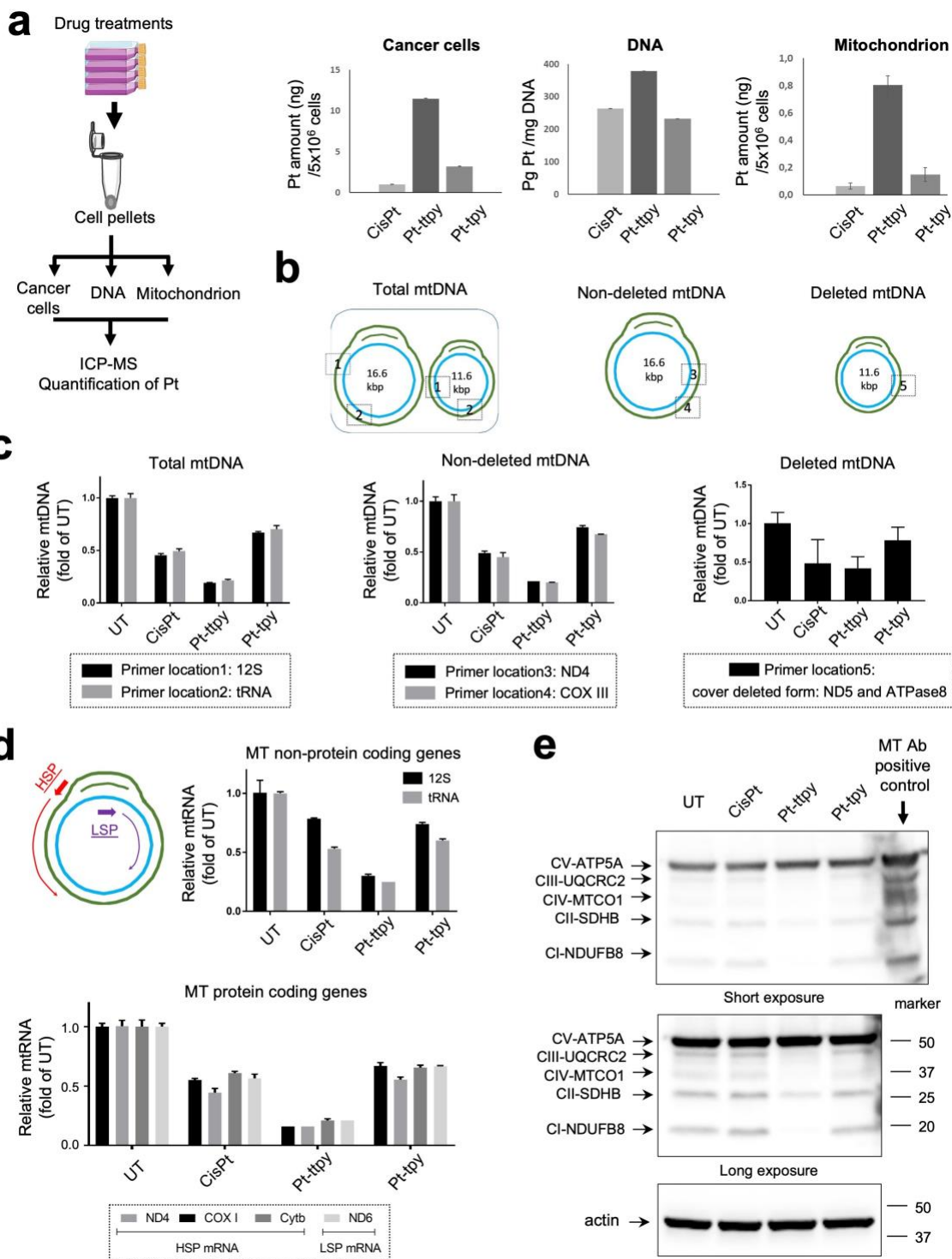
- 719 1. D. Varshney, J. Spiegel, K. Zyner, D. Tannahill, S. Balasubramanian, The regulation and
720 functions of DNA and RNA G-quadruplexes. *Nat Rev Mol Cell Biol* **21**, 459-474 (2020).
- 721 2. S. Neidle, Quadruplex nucleic acids as targets for anticancer therapeutics. *Nature Reviews*
722 *Chemistry* **1**, 0041 (2017).
- 723 3. J. L. Huppert, S. Balasubramanian, G-quadruplexes in promoters throughout the human
724 genome. *Nucleic Acids Res* **35**, 406-413 (2007).
- 725 4. A. Bedrat, L. Lacroix, J. L. Mergny, Re-evaluation of G-quadruplex propensity with
726 G4Hunter. *Nucleic Acids Res* **44**, 1746-1759 (2016).
- 727 5. V. S. Chambers *et al.*, High-throughput sequencing of DNA G-quadruplex structures in the
728 human genome. *Nat Biotechnol* **33**, 877-881 (2015).
- 729 6. R. Hansel-Hertsch *et al.*, G-quadruplex structures mark human regulatory chromatin. *Nat*
730 *Genet* **48**, 1267-1272 (2016).
- 731 7. D. Rhodes, H. J. Lipps, G-quadruplexes and their regulatory roles in biology. *Nucleic Acids*
732 *Res* **43**, 8627-8637 (2015).
- 733 8. S. L. Williams *et al.*, Replication-induced DNA secondary structures drive fork uncoupling
734 and breakage. *EMBO J* 10.15252/embj.2023114334, e114334 (2023).
- 735 9. M. Falabella, J. R. Fernandez, B. F. Johnson, A. B. Kaufman, Potential Roles for G-
736 Quadruplexes in Mitochondria. *Current Medicinal Chemistry* **26**, 2918-2932 (2019).
- 737 10. M. Doimo *et al.*, Enhanced mitochondrial G-quadruplex formation impedes replication
738 fork progression leading to mtDNA loss in human cells. *Nucleic Acids Res* **51**, 7392-7408
739 (2023).

- 740 11. S. Dahal, H. Siddiqua, V. K. Katapadi, D. Iyer, S. C. Raghavan, Characterization of G4 DNA
741 formation in mitochondrial DNA and their potential role in mitochondrial genome
742 instability. *The FEBS Journal* **289**, 163-182 (2022).
- 743 12. V. J. Sahayasheela, Z. Yu, T. Hidaka, G. N. Pandian, H. Sugiyama, Mitochondria and G-
744 quadruplex evolution: an intertwined relationship. *Trends Genet*
745 10.1016/j.tig.2022.10.006 (2022).
- 746 13. S. K. Bharti *et al.*, DNA sequences proximal to human mitochondrial DNA deletion
747 breakpoints prevalent in human disease form G-quadruplexes, a class of DNA structures
748 inefficiently unwound by the mitochondrial replicative Twinkle helicase. *J Biol Chem* **289**,
749 29975-29993 (2014).
- 750 14. M. J. Hannon, J. Reedijk, Metal interactions with nucleic acids. *Dalton Trans* **44**, 3503-3504
751 (2015).
- 752 15. R. Vilar, Nucleic Acid Quadruplexes and Metallo-Drugs. *Met Ions Life Sci* **18** (2018).
- 753 16. A. Garci *et al.*, Efficient and Rapid Mechanochemical Assembly of Platinum(II) Squares for
754 Guanine Quadruplex Targeting. *J Am Chem Soc* **139**, 16913-16922 (2017).
- 755 17. L. Y. Liu *et al.*, Organic-Platinum Hybrids for Covalent Binding of G-Quadruplexes:
756 Structural Basis and Application to Cancer Immunotherapy. *Angew Chem Int Ed Engl* **62**,
757 e202305645 (2023).
- 758 18. S. Neidle, Quadruplex nucleic acids as targets for anticancer therapeutics. *Nature Reviews*
759 *Chemistry* **56** (2017).
- 760 19. Z. Deng, G. Zhu, Beyond mere DNA damage: Recent progress in platinum(IV) anticancer
761 complexes containing multi-functional axial ligands. *Curr Opin Chem Biol* **74**, 102303
762 (2023).
- 763 20. Z. Yu *et al.*, Chem-map profiles drug binding to chromatin in cells. *Nat Biotechnol* **41**, 1265-
764 1271 (2023).
- 765 21. M. Falabella *et al.*, G-quadruplex dynamics contribute to regulation of mitochondrial gene
766 expression. *Sci Rep* **9**, 5605 (2019).
- 767 22. H. Bertrand *et al.*, The importance of metal geometry in the recognition of G-quadruplex-
768 DNA by metal-terpyridine complexes. *Org Biomol Chem* **5**, 2555-2559 (2007).
- 769 23. E. Morel *et al.*, Selectivity of Terpyridine Platinum Anticancer Drugs for G-quadruplex DNA.
770 *Molecules* **24** (2019).
- 771 24. H. Bertrand *et al.*, Exclusive platination of loop adenines in the human telomeric G-
772 quadruplex. *Org Biomol Chem* **7**, 2864-2871 (2009).
- 773 25. M. Trajkovski *et al.*, Interactions of Pt-ttpty with G-Quadruplexes Originating from
774 Promoter Region of the c-myc Gene Deciphered by NMR and Gel Electrophoresis Analysis.
775 *Chemistry* **21**, 7798-7807 (2015).
- 776 26. L. Saker *et al.*, Platinum Complexes Can Bind to Telomeres by Coordination. *Int J Mol Sci*
777 **19** (2018).
- 778 27. H. S. Lee *et al.*, Systematic Analysis of Compounds Specifically Targeting Telomeres and
779 Telomerase for Clinical Implications in Cancer Therapy. *Cancer Res* **78**, 6282-6296 (2018).
- 780 28. S. Ali *et al.*, Pt-ttpty, a G-quadruplex binding platinum complex, induces telomere
781 dysfunction and G-rich regions DNA damage. *Metallomics* **13** (2021).
- 782 29. A. Erxleben, Mitochondria-Targeting Anticancer Metal Complexes. *Curr Med Chem* **26**,
783 694-728 (2019).
- 784 30. O. Rothfuss, T. Gasser, N. Patenge, Analysis of differential DNA damage in the
785 mitochondrial genome employing a semi-long run real-time PCR approach. *Nucleic Acids*
786 *Res* **38**, e24 (2010).
- 787 31. Z. Zhu *et al.*, Mitochondrion-targeted platinum complexes suppressing lung cancer
788 through multiple pathways involving energy metabolism. *Chem Sci* **10**, 3089-3095 (2019).
- 789 32. M. Reers, T. W. Smith, L. B. Chen, J-aggregate formation of a carbocyanine as a quantitative
790 fluorescent indicator of membrane potential. *Biochemistry* **30**, 4480-4486 (1991).

- 791 33. S. T. Smiley *et al.*, Intracellular heterogeneity in mitochondrial membrane potentials
792 revealed by a J-aggregate-forming lipophilic cation JC-1. *Proc Natl Acad Sci U S A* **88**, 3671-
793 3675 (1991).
- 794 34. I. Vercellino, L. A. Sazanov, The assembly, regulation and function of the mitochondrial
795 respiratory chain. *Nat Rev Mol Cell Biol* **23**, 141-161 (2022).
- 796 35. A. P. Leonard *et al.*, Quantitative analysis of mitochondrial morphology and membrane
797 potential in living cells using high-content imaging, machine learning, and morphological
798 binning. *Biochim Biophys Acta* **1853**, 348-360 (2015).
- 799 36. D. B. Zorov, M. Juhaszova, S. J. Sollott, Mitochondrial ROS-induced ROS release: an update
800 and review. *Biochim Biophys Acta* **1757**, 509-517 (2006).
- 801 37. M. Kleih *et al.*, Direct impact of cisplatin on mitochondria induces ROS production that
802 dictates cell fate of ovarian cancer cells. *Cell Death Dis* **10**, 851 (2019).
- 803 38. S. Rath *et al.*, MitoCarta3.0: an updated mitochondrial proteome now with sub-organelle
804 localization and pathway annotations. *Nucleic Acids Res* **49**, D1541-D1547 (2021).
- 805 39. C. Li *et al.*, Ligand-induced native G-quadruplex stabilization impairs transcription
806 initiation. *Genome Res* **31**, 1546-1560 (2021).
- 807 40. J. Shen *et al.*, Promoter G-quadruplex folding precedes transcription and is controlled by
808 chromatin. *Genome Biol* **22**, 143 (2021).
- 809 41. C. Estell, E. Stamatidou, S. El-Messeiry, A. Hamilton, In situ imaging of mitochondrial
810 translation shows weak correlation with nucleoid DNA intensity and no suppression
811 during mitosis. *J Cell Sci* **130**, 4193-4199 (2017).
- 812 42. Q. Zhang, Q. B. Lu, New combination chemotherapy of cisplatin with an electron-donating
813 compound for treatment of multiple cancers. *Sci Rep* **11**, 788 (2021).
- 814 43. C. Tang, M. J. Livingston, R. Safirstein, Z. Dong, Cisplatin nephrotoxicity: new insights and
815 therapeutic implications. *Nat Rev Nephrol* **19**, 53-72 (2023).
- 816 44. P. K. Kopinski, L. N. Singh, S. Zhang, M. T. Lott, D. C. Wallace, Mitochondrial DNA variation
817 and cancer. *Nat Rev Cancer* **21**, 431-445 (2021).
- 818 45. S. P. Wisnovsky *et al.*, Targeting mitochondrial DNA with a platinum-based anticancer
819 agent. *Chem Biol* **20**, 1323-1328 (2013).
- 820 46. Y. Guo *et al.*, Enhancing Cytotoxicity of a Monofunctional Platinum Complex via a Dual-
821 DNA-Damage Approach. *Inorg Chem* **58**, 13150-13160 (2019).
- 822 47. D. Gibson, Platinum(IV) anticancer agents; are we en route to the holy grail or to a dead
823 end? *J Inorg Biochem* **217**, 111353 (2021).
- 824 48. I. C. Summerhayes *et al.*, Unusual retention of rhodamine 123 by mitochondria in muscle
825 and carcinoma cells. *Proc Natl Acad Sci U S A* **79**, 5292-5296 (1982).
- 826 49. D. Varshney *et al.*, RNA G-quadruplex structures control ribosomal protein production.
827 *Scientific Reports* **11**, 22735 (2021).
- 828 50. H. J. Kim, P. Maiti, A. Barrientos, Mitochondrial ribosomes in cancer. *Semin Cancer Biol* **47**,
829 67-81 (2017).
- 830 51. S. Bao *et al.*, Potential of Mitochondrial Ribosomal Genes as Cancer Biomarkers
831 Demonstrated by Bioinformatics Results. *Front Oncol* **12**, 835549 (2022).
- 832 52. S. Dasari, P. B. Tchounwou, Cisplatin in cancer therapy: molecular mechanisms of action.
833 *Eur J Pharmacol* **740**, 364-378 (2014).
- 834 53. V. Gandin, J. D. Hoeschele, N. Margiotta, Special Issue "Cisplatin in Cancer Therapy:
835 Molecular Mechanisms of Action 3.0". *Int J Mol Sci* **24** (2023).
- 836 54. R. Marullo *et al.*, Cisplatin induces a mitochondrial-ROS response that contributes to
837 cytotoxicity depending on mitochondrial redox status and bioenergetic functions. *PLoS*
838 *One* **8**, e81162 (2013).
- 839 55. R. Oun, Y. E. Moussa, N. J. Wheate, The side effects of platinum-based chemotherapy
840 drugs: a review for chemists. *Dalton Trans* **47**, 6645-6653 (2018).
- 841 56. X. Xie *et al.*, Pyrocatechol Alleviates Cisplatin-Induced Acute Kidney Injury by Inhibiting
842 ROS Production. *Oxid Med Cell Longev* **2022**, 2158644 (2022).

- 843 57. M. E. Kauffman *et al.*, MitoSOX-Based Flow Cytometry for Detecting Mitochondrial ROS.
844 *React Oxyg Species (Apex)* **2**, 361-370 (2016).
- 845 58. A. F. Phillips *et al.*, Single-Molecule Analysis of mtDNA Replication Uncovers the Basis of
846 the Common Deletion. *Mol Cell* **65**, 527-538 e526 (2017).
- 847 59. A. Panday, R. Elango, N. A. Willis, R. Scully, A modified CUT&RUN-seq technique for qPCR
848 analysis of chromatin-protein interactions. *STAR Protoc* **3**, 101529 (2022).
- 849
- 850

851 **Figures and Tables**



852

853

854

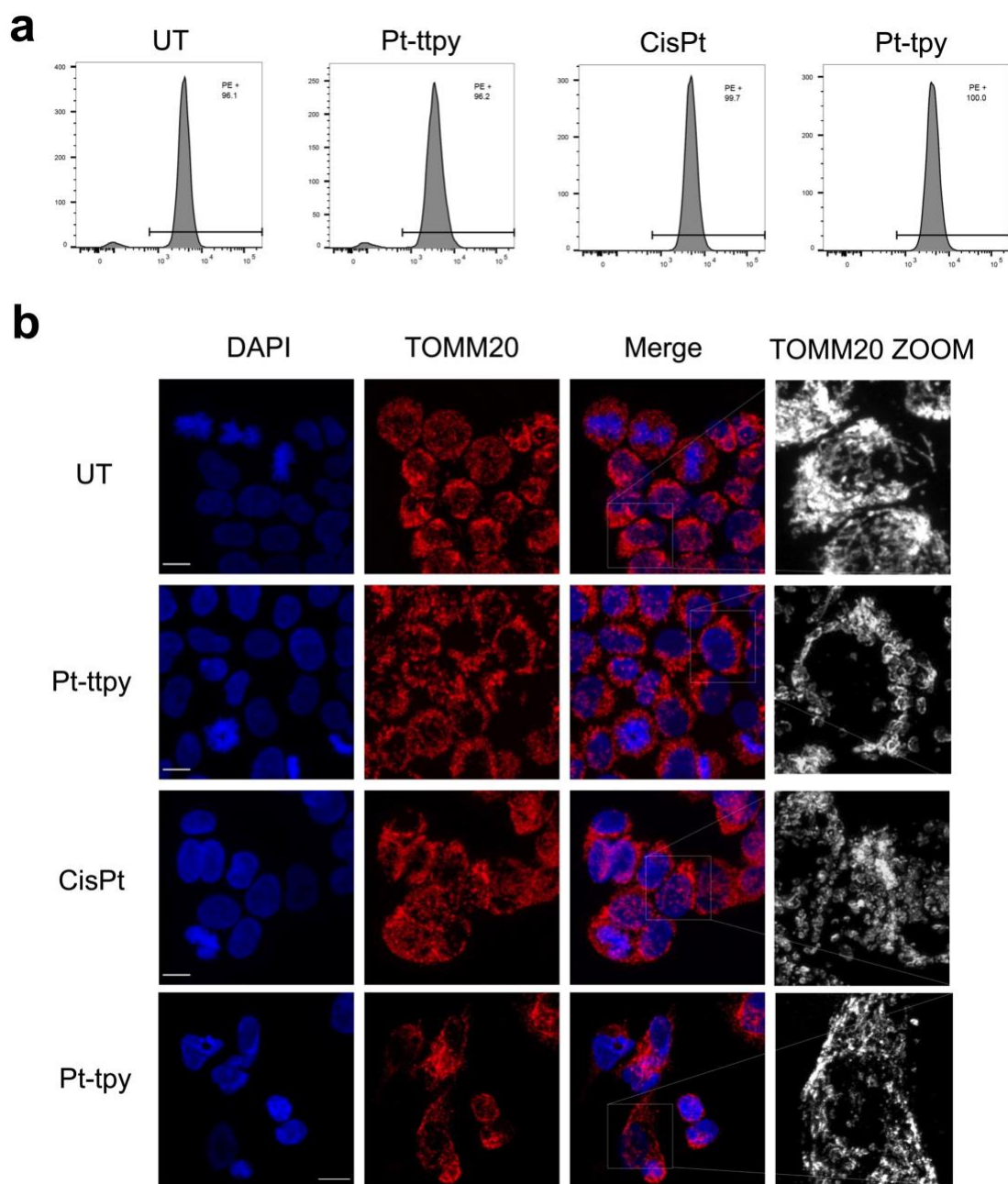
855

856

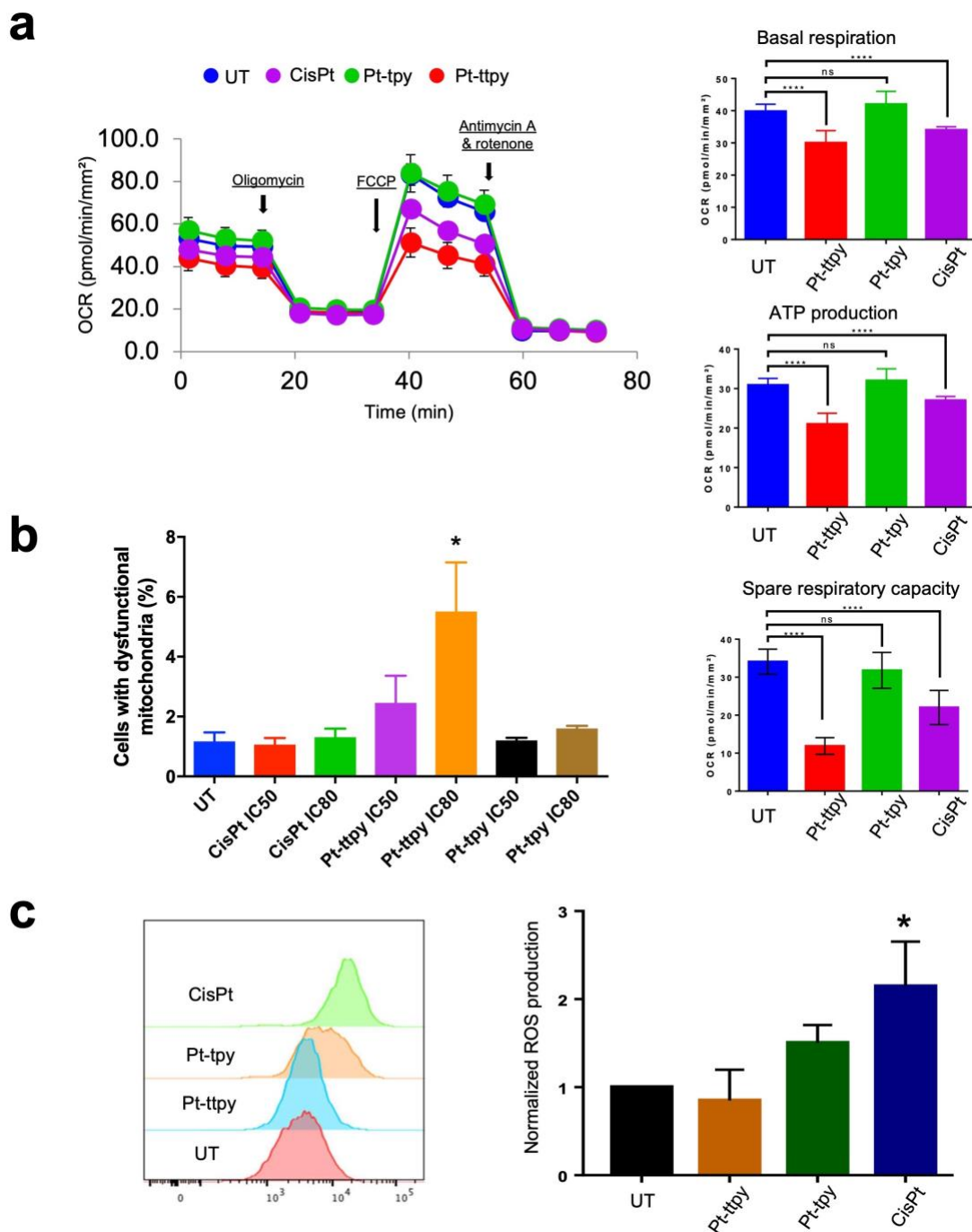
Figure 1. Impact of different platinum (Pt) complexes (cisplatin, Pt-ttpy and Pt-tpy) on cellular uptake and distribution with the potential toxicity to mitochondrial genome at their IC₈₀ concentration in A2870 treated cells. (a) Schematic illustration of platinum quantification flow in cell pellets, genomic DNA and mitochondria is presented in the left, comparative quantification of Pt

857 amount(ng)/5x10⁶ cells for cisplatin, Pt-ttpy and Pt-tpy was performed in cell pellet, extracted
858 genomic DNA and isolated mitochondria, respectively after 96 hours treatment. Data represents
859 three independent experiments with the mean ± SEM. (b) a sketch of describing different primers'
860 position in non-deleted mt-DNA, deleted mt-DNA and total mt-DNA is presented, that is used for
861 qPCR analysis as presented in figure (c). (c) qPCR quantification of different mt-DNA copy numbers
862 under different Pt complexes treatments after 96 hours treatment, data is presented as relative fold
863 changes of mtDNA copy numbers for different Pt complexes' treatment groups compared to the
864 untreated (UT) group. Data represents three independent experiments with the mean ± SEM. (d)
865 RT-qPCR quantification of different mt-RNA levels, including both mt non-protein coding genes and
866 its protein coding genes in response to different Pt complexes' 96h treatment groups compared to
867 the UT group. Data represents three independent experiments with the mean ± SEM. (e) Western
868 blot study of different mt OXPHOS complex proteins in the 96 hours treatment of different Pt
869 complexes. Also shown is a blot of actin as a loading control. The corresponding quantification data
870 of different mt OXPHOS complex protein levels is presented in the supplementary figure 2. Data
871 represents two independent experiments.

872



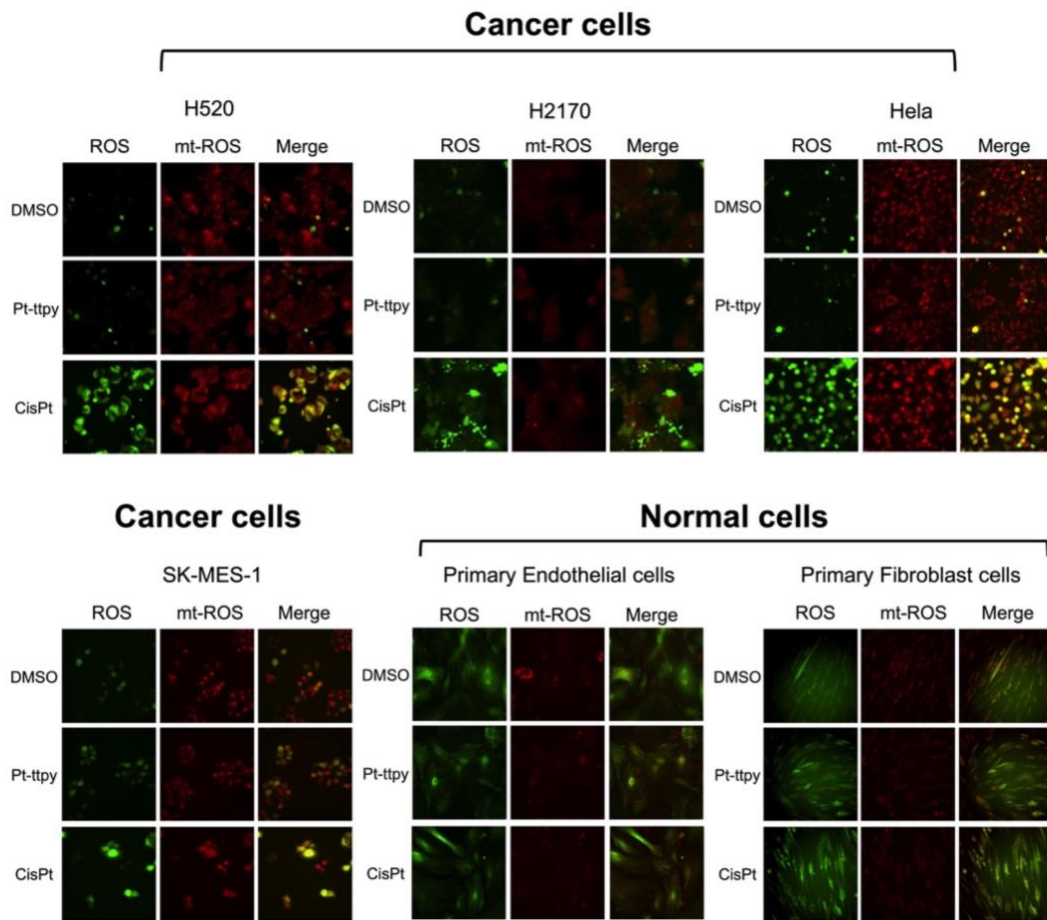
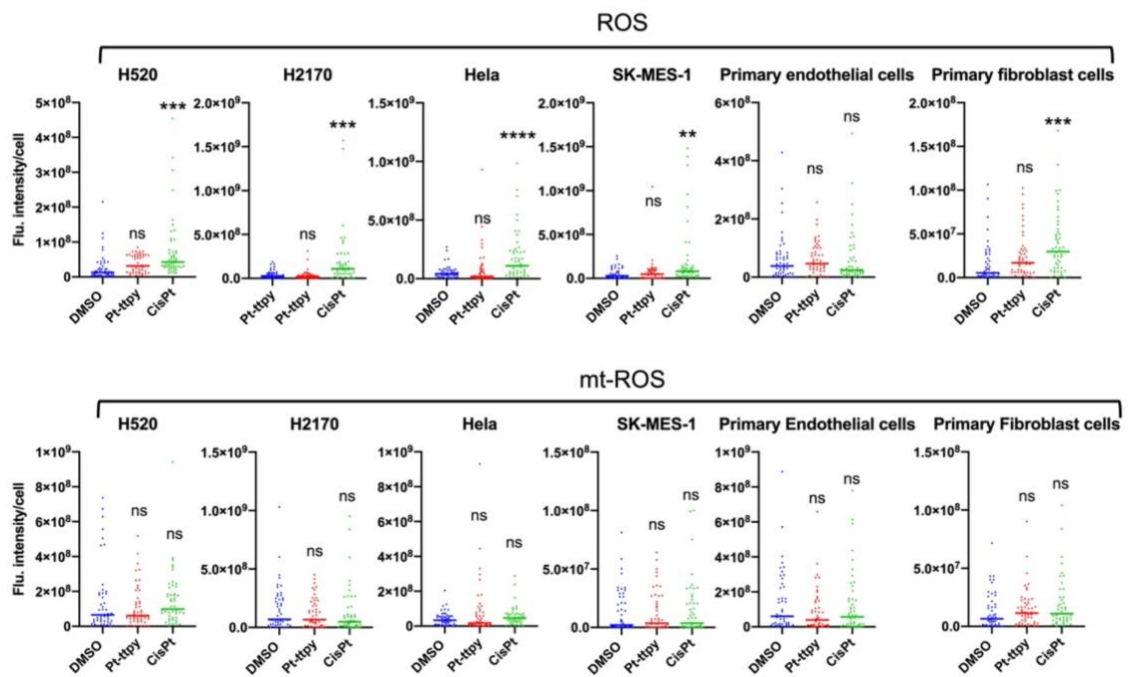
873
 874 **Figure 2.** Impact of three platinum (Pt) complexes (cisplatin, Pt-ttpy and Pt-tpy) in mitochondrial
 875 number and its morphology of A2870 treated cells. (a) Flow cytometry analysis of mitochondrial
 876 number changes in the treatment of different Pt complexes by the staining of TOMM20, plotted are
 877 the TOMM20 signal distribution in different treatments. The histogram is represented by two
 878 independent experiments. (b) Confocal microscope tested the mitochondrial abundance and its
 879 morphology changes following the Pt complexes treatments (cisplatin, Pt-ttpy and Pt-tpy) for 96h.
 880 Scale bar: 10µm. Data represents three independent experiments.
 881



882
883

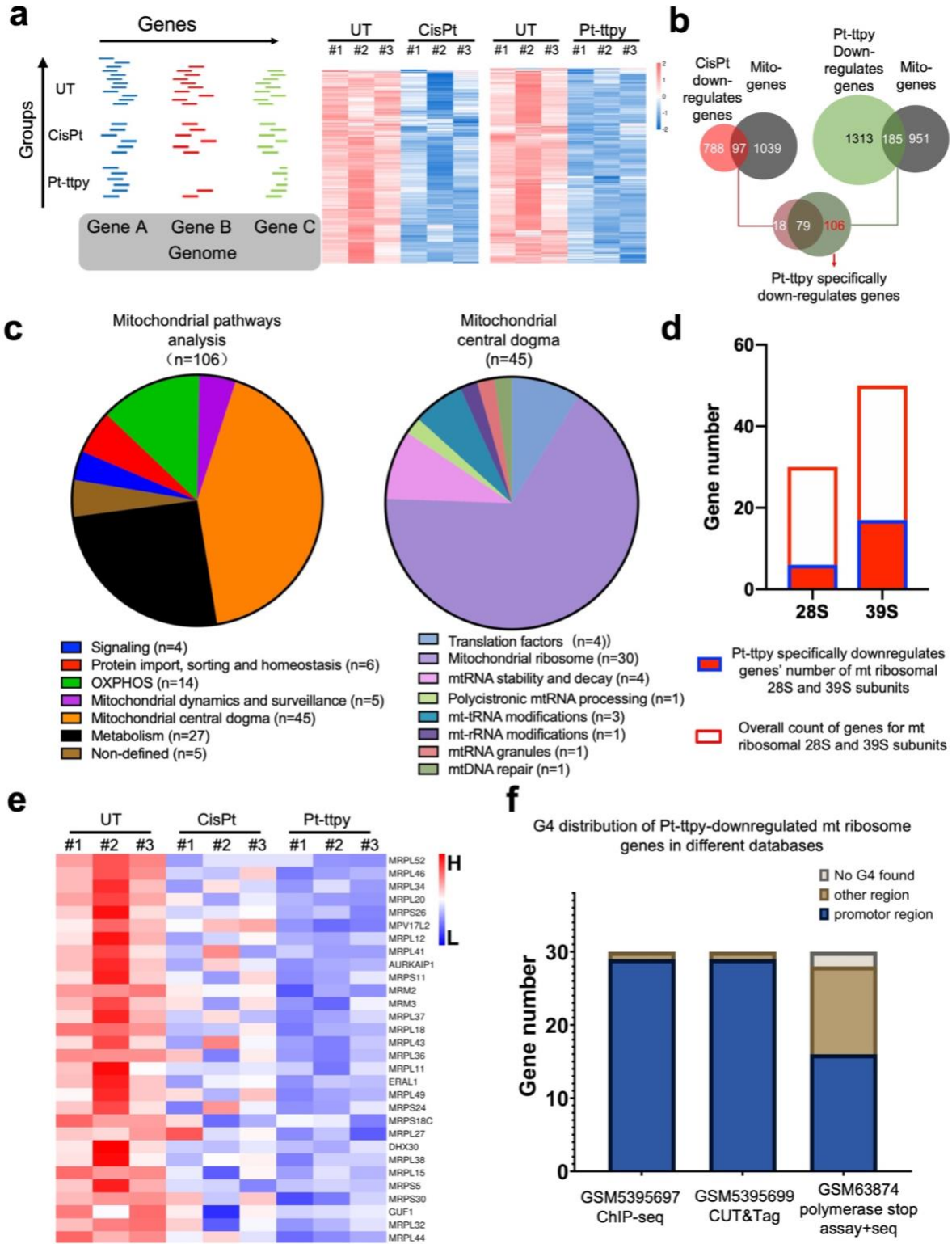
884 **Figure 3.** Impact of three platinum (Pt) complexes (cisplatin, Pt-tpy and Pt-tpy) on mitochondrial
885 homeostasis in A2870 treated cells. (a) Left is presented as the seahorse XF cell mito stress test
886 profile under different Pt complexes treatments (10 μ M, 24h treatment) as well as UT group with
887 specific electron transport chain inhibitors: oligomycin (inhibitor of ATP synthase (complex V)),
888 FCCP (uncoupling agent), antimycin-A (complex III inhibitor), and rotenone (complex I inhibitor).
889 Right is plotted as the quantification of basal respiration, ATP production and spare respiratory
890 capacity respectively by different treatments of Pt complexes. (b) Flow cytometry was used to

891 quantify mitochondrial potential changes by the staining of JC1, % Cells with mitochondrial
892 membrane loss (dysfunctional mitochondria) corresponding to the % of cells with JC-1 in its green
893 monomers form after treatment at the respective IC₅₀ and IC₈₀ concentrations of the complexes.
894 Data represents three independent experiments with the mean ± SEM. (c) Flow cytometry was
895 used to quantify the total ROS production in A2870 cells treated, normalized ROS production is
896 plotted as the mean ± SEM, data represents three independent experiments. P values were
897 calculated toward the UT: *P < 0.05, **P < 0.01, ****P < 0.0001, unpaired t-Student test.
898

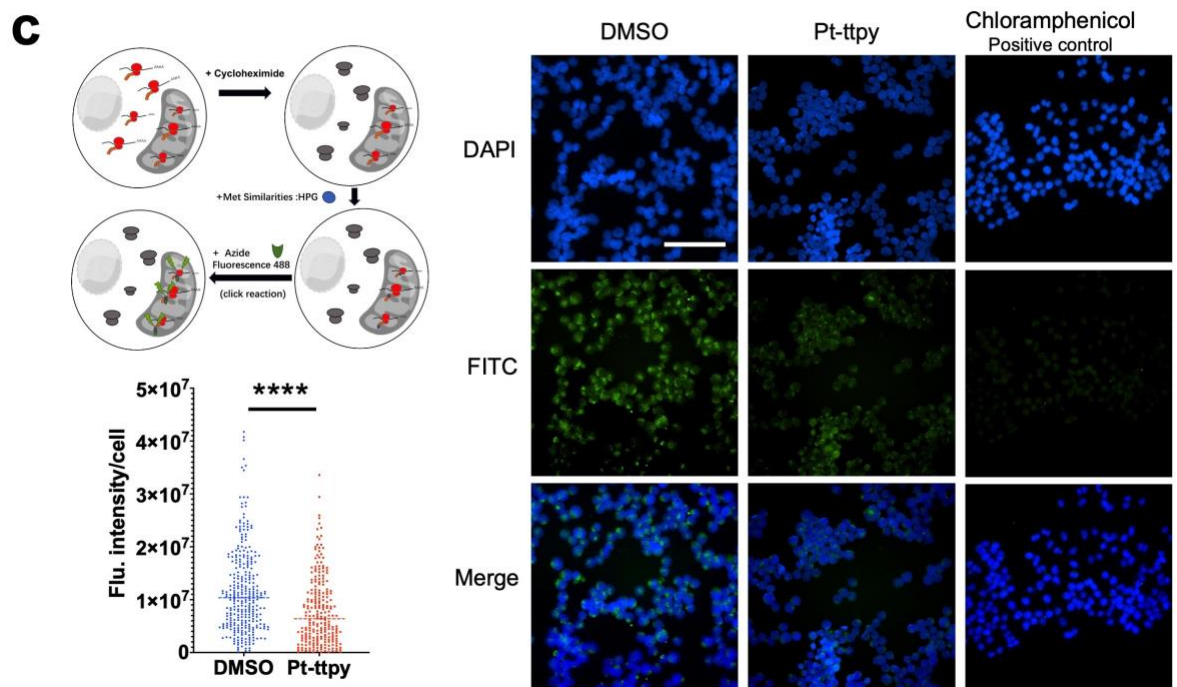
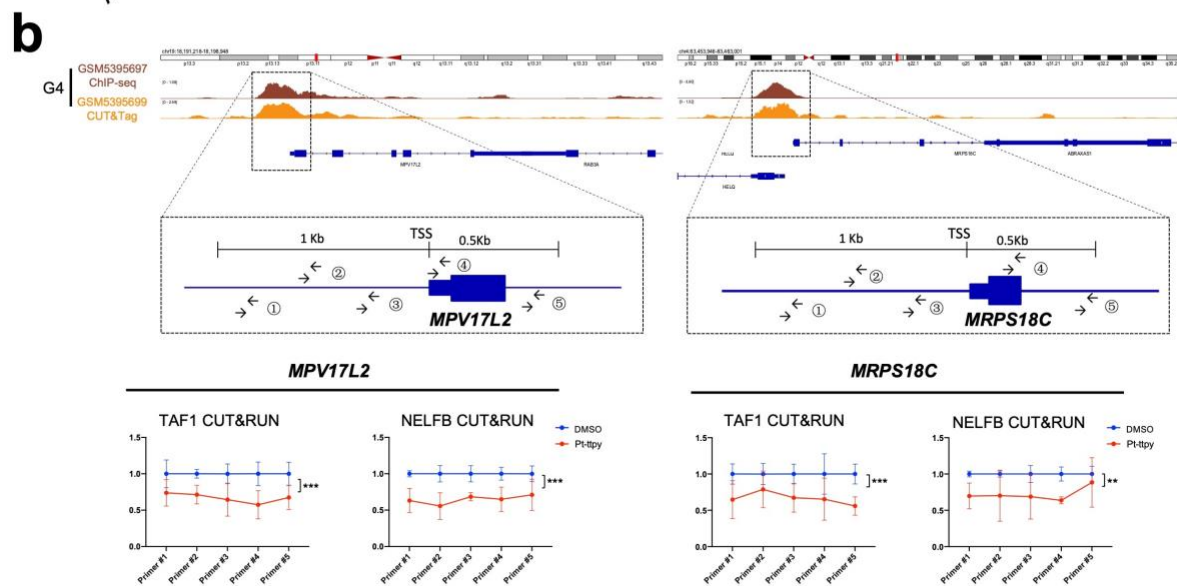
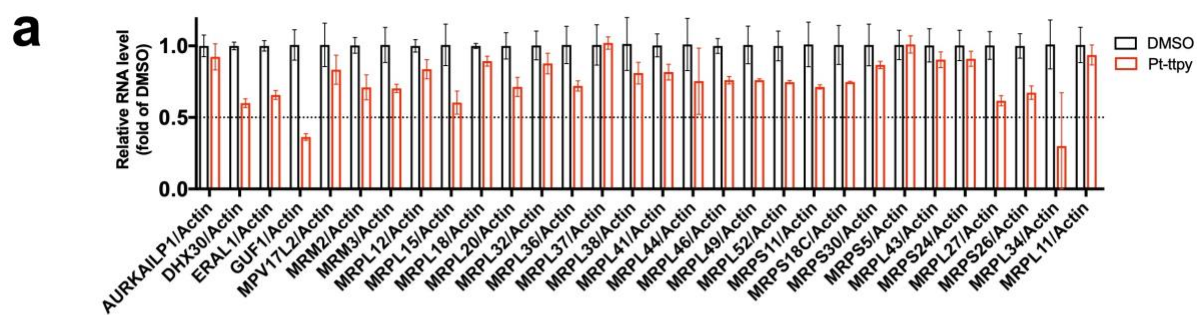
a**b**

900 **Figure 4.** Fluorescence screening of Pt-ttpy and cisplatin effects on ROS and mitochondrial ROS
901 (mt-ROS) induction with single cell fluorescence intensity quantification in four different cancer cell
902 lines and two primary cells (Endothelial cells and Fibroblast cells) post DMSO, Pt-ttpy or cisplatin
903 treatments. (a) represented figures of fluorescent imaging of different cell (line) under Pt-ttpy and
904 cisplatin treatments for 24 h at either 10 μ M (for cancer cells) or 1 μ M (for primary cells). The general
905 ROS production was detected by green channel (ex: 488nm), the mitochondrial specific ROS (mt-
906 ROS) production was detected by red channel (ex: 621nm). (b) The single cell fluorescence
907 quantification for both ROS and mt-ROS in different cell (lines) post indicated treatments was
908 performed by Image J using in-house developed Macros, DMSO group (n>50), Pt-ttpy group
909 (n>50), cisplatin group (n>50). Line indicates the median flu. intensity, P values were calculated
910 toward the DMSO group: *P < 0.05, **P < 0.01, ****P < 0.0001, unpaired t-Student test.

911



914 **Figure 5.** Pt-tpty show preferable inhibition of mitochondrial ribosome-related gene expression by
915 RNA seq, as compared with cisplatin treatment of A2780 cells for 96h at their IC₈₀ concentration,
916 respectively. (a) Left: Schematic illustration of RNA seq under different treatments, heatmap
917 showcasing the down-regulated gene expression under cisplatin and Pt-tpty treatments, as
918 compared with the UT group. Each group has three biological replicates. (b) A sketch of the
919 procedural flow of data mining is aiming at identifying mitochondrial genes specifically down-
920 regulated by Pt-tpty. (c) Left: Analysis of mitochondrial pathways indicates that Pt-tpty-specifically
921 down-regulated genes (106 genes) exhibit high enrichment within the mitochondrial central dogma
922 (45/106) (38). Right: these genes predominantly impact the expression of mitochondrial ribosome
923 genes (30/45). This analysis employed the MitoCarta3.0_MitoPathways tool (38). (d) Plotting of
924 gene number distribution for mitochondrial ribosome genes specifically down-regulated by Pt-tpty
925 and the overall count of genes for mitochondrial ribosome 28S and 39S subunits (e) A heatmap
926 analysis was conducted to visualize the expression levels of mitochondrial ribosome genes
927 specifically down-regulated by Pt-tpty in the UT, cisplatin, and Pt-tpty treatment groups. The data
928 was sorted and visualized by raw-normalized values. (f) Pt-tpty specifically downregulates mt
929 ribosome genes show high enrichment of G4 distribution mostly in the promoter region from various
930 databases (5, 39).
931

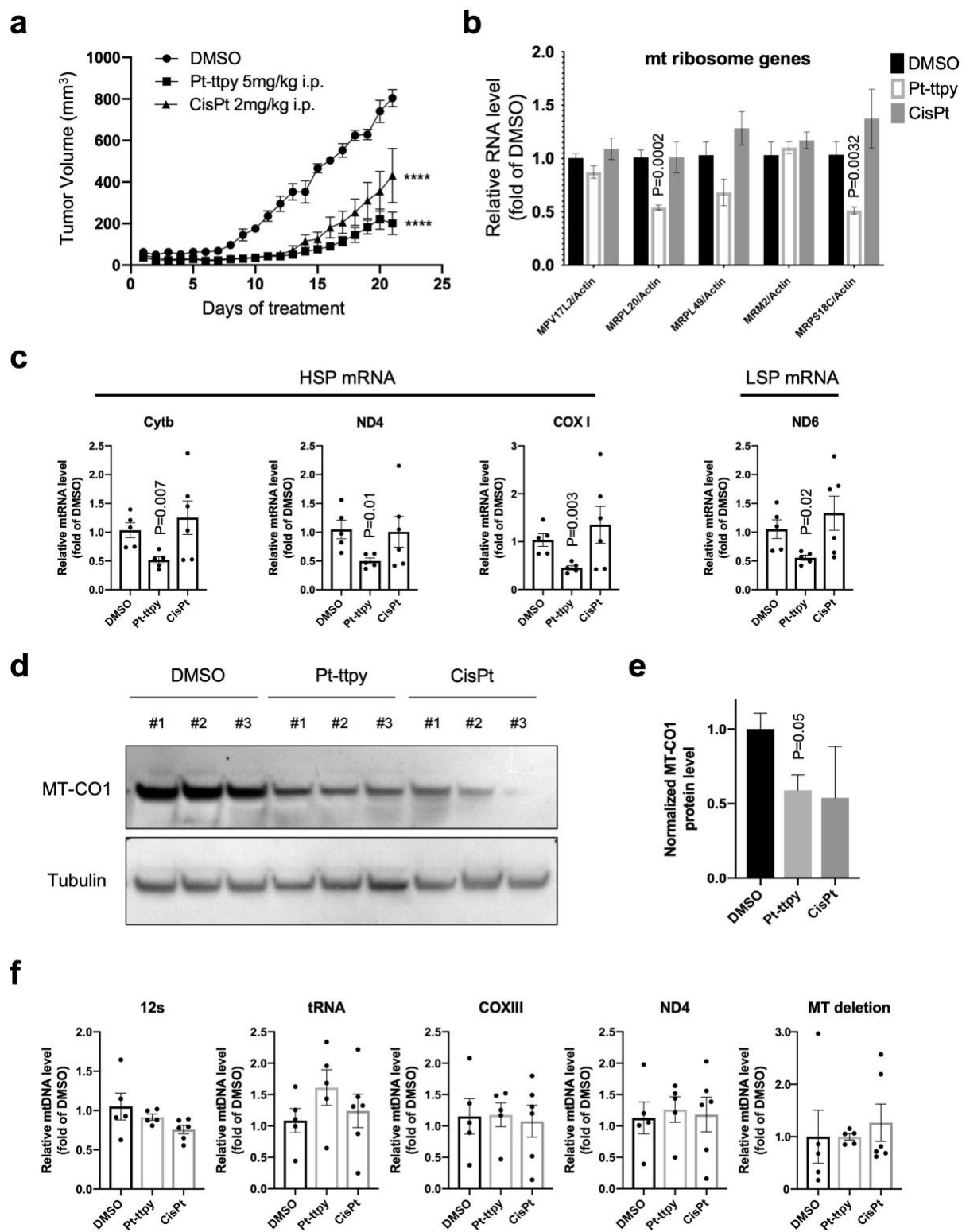


932

31

933 **Figure 6.** Pt-ttpty impairs G4 high enriched nuclear-encoded mt ribosome genes' transcription
934 initiation and elongation and dampens specific mt ribosome function of translation in A2780 treated
935 cells. (a) RT-qPCR experiments confirmed Pt-ttpty show a broad inhibition of MT ribosome gene
936 expression. Data is represented as mean \pm SEM (n=3). (b) Up: IGV visualization of *MPV17L2* and
937 *MRPS18C* genes containing high abundance of G4 sequences in the TSS regions from the latest
938 DNA G4 databases (39). And five pairs of primers were designed in around 1.5Kb TSS region and
939 CUT&RUN experiments were performed to detect transcription and elongation factors binding.
940 Down: Pt-ttpty significantly reduced the occupancy of TAF1 (general transcription factor TFIID
941 subunit) and NELFB (Pol II-associated NELF complex member B) at the promoter and its
942 surrounded regions of mt ribosome genes *MPV17L2* and *MRPS18C*. The data were expressed as
943 the mean \pm SEM (n=3). P values were calculated by 2way ANOVA analysis between DMSO and
944 Pt-ttpty groups: *P < 0.05, **P < 0.01, ****P < 0.0001. (c) Left up: Schematic illustration of studying
945 flow of mt ribosome function by the Click-chemistry based IF assay. Left: down: Single-cell
946 quantification showed Pt-ttpty significantly inhibited mitochondrial translation, DMSO group (>200),
947 Pt-ttpty group (n>200). Data represents three independent experiments. Right: represented figures
948 of fluorescent imaging of the mitochondria under Pt-ttpty and DMSO treatments. A Positive control
949 of blocking the synthesis of mitochondrial proteins by chloramphenicol was also presented. Line
950 indicates the median Flu. intensity value, P values were calculated toward the DMSO group: *P <
951 0.05, **P < 0.01, ****P < 0.0001, unpaired t-Student test.

952



953

33

954 **Figure 7.** *In vivo*: A2780 nude mice xenograft tumor model suggests that Pt-ttpty, not cisplatin,
955 significantly inhibits the mRNA levels of both nuclear-encoded mt ribosome genes expression and
956 mt both light and heavy chains-encoded genes and downregulates mt protein MT-CO1 by tumor
957 tissue samples, DMSO group (n=5), Pt-ttpty group (n=5), and cisplatin group (n=6). (a) Tumor
958 growth curves of nude mice under the treatments of DMSO, Pt-ttpty and cisplatin, respectively (b)
959 RT-qPCR quantification of mRNA levels of mitochondrial ribosome-related genes in tumor tissues.
960 (c) RT-qPCR quantification of mRNA levels of genes-encoded by both mitochondrial light and
961 heavy chains. (d) Western blot results of MT-CO1 Protein expression levels, n=3. (e) Graph show
962 the quantification of MT-CO1 protein levels after normalizing the data to DMSO group. (f) q-PCR
963 quantification of mt gene copy number changes by different primers located in different mt gene
964 region in tumor tissues. Data are expressed as mean \pm SEM of three biological replicates. P values
965 were calculated by unpaired t-test: *P < 0.05, **P < 0.01, ****P < 0.0001.

966

Supporting Information for

A G-quadruplex-binding platinum complex induces cancer mitochondrial dysfunction *in vitro* and *in vivo* independently of ROS induction

Keli Kuang^{a1}, Chunyan Li^{a1}, Fatlinda Maksut^{b,c}, Deepanjan Ghosh^{b,c}, Robin Vinck^d, Maoling Wang^a, Joël Poupon^e, Run Xiang^f, Wen Li^g, Fei Li^a, Zhu Wang^a, Junrong Du^a, Marie-Paule Teulade-Fichou^{b,c}, Gilles Gasser^d, Sophie Bombard^{b,c*} and Tao Jia^{a,b,c*}

- a Key Laboratory of Drug-Targeting and Drug Delivery System of the Education Ministry and Sichuan Province, Sichuan Engineering Laboratory for Plant-Sourced Drug and Sichuan Research Center for Drug Precision Industrial Technology, West China School of Pharmacy, Sichuan University, Chengdu 610041, China.
- b CNRS-UMR9187, INSERM U1196, PSL-Research University, 91405 Orsay, France
- c CNRS-UMR9187, INSERM U1196, Université Paris Saclay, 91405 Orsay, France
- d Chimie ParisTech, PSL University, CNRS, Institute of Chemistry for Life and Health Sciences, Laboratory for Inorganic Chemical Biology, F-75005 Paris, France.
- e Hôpital Lariboisière (AP-HP), Laboratoire de Toxicologie Biologique, 2 rue Ambroise Paré, 75475 Paris, France
- f Department of Thoracic Surgery, Sichuan Clinical Research Center for Cancer, Sichuan Cancer Hospital & Institute, Sichuan Cancer Center, Affiliated Cancer Hospital of University of Electronic Science and Technology of China, Chengdu, China.
- g Department of Medical Oncology, Cancer Center, West China Hospital, Sichuan University, Chengdu, China

Keli Kuang¹ and Chunyan Li¹ are considered joint first author.

*Corresponding author:

Tao Jia* **Email:** taojia86@scu.edu.cn;

Sophie Bombard* **Email:** Sophie.bombard@curie.fr

This PDF file includes:

Supporting text
Figures S1 to S11
Tables S1
SI References

Supporting Information Text

Materials and Methods

qPCR-based method for detection of the mt DNA lesion

Investigating mitochondrial DNA (mtDNA) damage in the treatment of different metallic complexes at their IC_{80} concentrations for 96 hours was performed as previously described protocol (1). Generally, total DNA was purified using DNA Blood and Tissue Kit (Qiagen, Germany) from cells under indicated drug treatments. DNA quantity was determined by NanoDrop (Thermo Fisher). The isolated DNA showed a high purity ($A_{260}/A_{280} > 1.8$) and was stored at $-20^{\circ}C$. The primers used for real time amplification were synthesized and HPLC-purified by Eurogentec. The primers used in this study are the ones allowing to detect mtDNA lesion in the region opposite to the D-loop which is a partially relaxed structures and consequently more fragile than other mt-DNA region: Short amplicon primers Forward: CATGCCCATCGTCCTAGAAT, Short amplicon primers Reverse: ACGGGCCCTATTTCAAAGAT; Long amplicon primers Forward: CATGCCCATCGTCCTAGAAT, Long amplicon primers Reverse: TGTTGTCTGCAGGTAGAGG. Briefly, the PCR conditions to run long and short fragments by QuantStudio 5 real-time PCR system and the mt-DNA damage calculated as lesion per 10 kb DNA of each mt-DNA region were performed in the same manner as previously reported (1). The real-time-PCR amplification of mitochondrial DNA fragments used to detect mtDNA lesions is sensitive enough to detect 8 oxo-G induced by ROS. Consequently, the mtDNA lesions detected by cisplatin treatment could be the consequence of ROS production. In contrast, for the Pt-tpy treatment, in the absence of ROS production, we can suggest that mtDNA lesions could be attributed to direct Pt-tpy adducts.

Mitochondrial membrane potential assay (JC-1 assay)

Changes in the mitochondrial potential were detected by 5,5,6,6-tetrachloro-1,10,3,3,3-tetraethylbenzimidazolylcarbocyanine iodide/chloride (JC-1, Biotium), a cationic dye that exhibits potential dependent accumulation in mitochondria, indicated by fluorescence emission shift from red (590 nm) to green (525 nm). A2780 cells were treated with various concentrations of cisplatin, Pt-tpy or Pt-tpy. After 96 hours treatment, cells were re-suspended 0.5 mL of PBS containing 2 μM final concentration of JC-1 probe and incubated at $37^{\circ}C$ for 15 min. After washing, cells were re-suspended in PBS and analysis was performed on a BD FACSCanto II cytometer. Mitochondria containing red JC-1 aggregates in healthy cells are detectable in the PE or PI channel, and green JC-1 monomers in apoptotic cells are detectable in FITC channel.

Annexin V apoptosis detection assay with 7-AAD

The A2780 cells were plated in a 6-well plate (100 000 cells) with indicated metallic complexes Pt-tpy cisplatin and Pt-tpy at their IC_{80} concentration for 96 hours. A2780 cell death has been assessed by Annexin V-FITC and 7-AAD incorporation (Biolegend) according to the manufacturer's instructions. Flow cytometry acquisitions were obtained on a FACSCanto IITM analyzer (BD Biosciences) with the assistance of BD FACSDiva Software (BD Biosciences) and data analyzed with the FlowJo Software (Tree Star).

Statistical analysis

The data were analyzed using Graphpad Prism 9.0 software (San Diego, CA). The results were presented as either mean \pm SEM or \pm SD as indicated, details of regarding the number of experimental replicates and statistical analyses methods were indicated in the figure legends.

Figures and Table

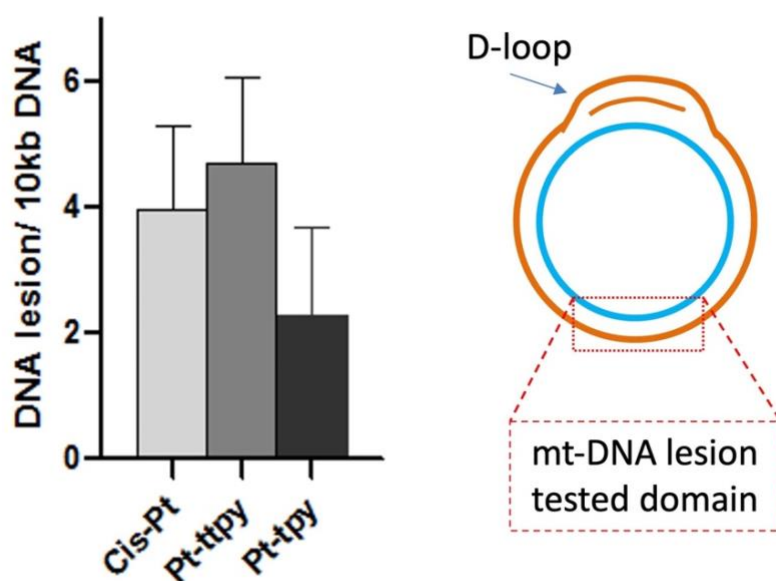


Fig. S1. Pt-tpy does not induce significant more DNA damage in mitochondrial genome by a semi-long run real-time PCR approach (1). Quantification of mitochondrial DNA lesion per 10 kb DNA by SLR rt-PCR amplification of total DNA isolated from A2780 cells treated by Pt-ttpty, Pt-tpy and cisplatin at their IC_{80} con. for 96h in the indicated domain.

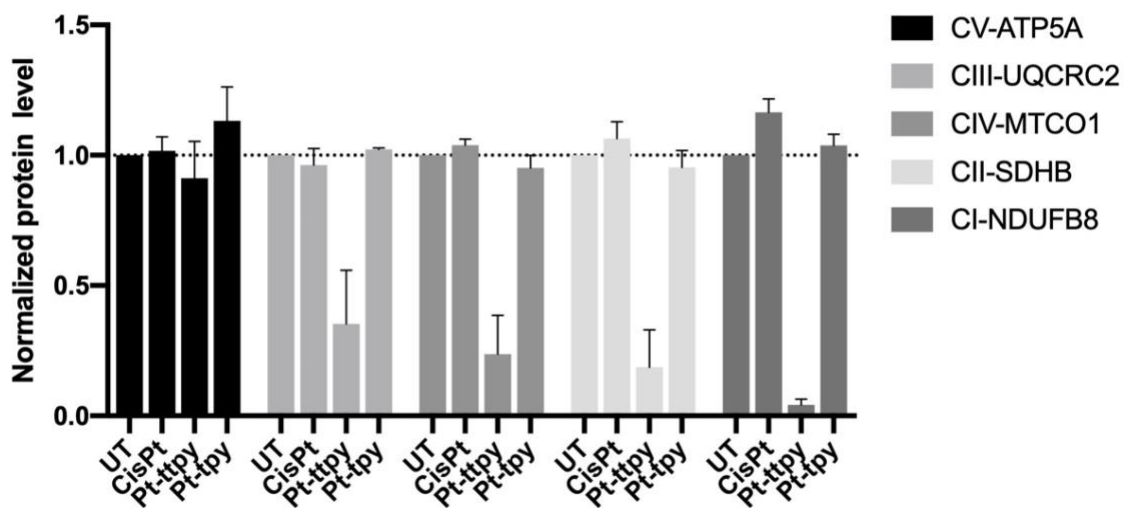


Fig. S2. Protein quantification of different MT OXPHOS complex proteins in the treatment of A2780 with the three Pt complexes (cisplatin, Pt-ttpy and Pt-tpy). Data is represented by two independent experiments with mean \pm SEM.

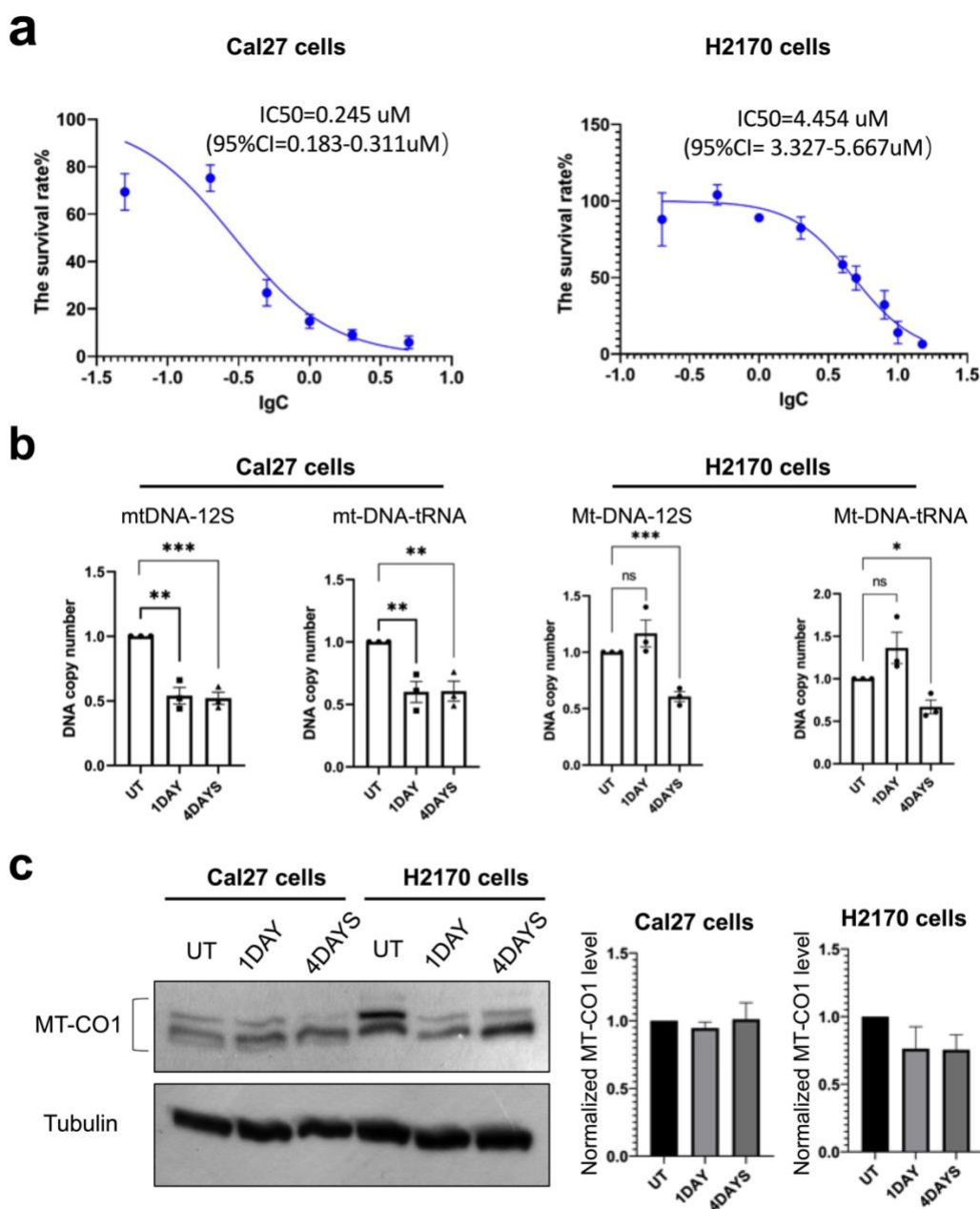


Fig. S3. Impact of Pt-ttpy effects on mitochondrial DNA copy number and mitochondria-encoded protein MT-CO1 protein level. (a) IC₅₀ determination of Pt-ttpy in cancer cells Cal27 and H2170 respectively. Data represents three independent experiments with the mean \pm SEM (b) qPCR quantification of different mt-DNA copy number changes under Pt-ttpy treatment in Cal27 and H2170 cells at their respective IC₈₀ concentration after 1day and 4days treatments, data is presented as relative fold changes of mtDNA copy numbers for Pt-ttpy group compared to the untreated (UT) group. Data represents three independent experiments with the mean \pm SEM. P values were calculated toward the UT: *P < 0.05, **P < 0.01, ****P < 0.0001, unpaired t-Student test. (c) left: western blot study of MT-CO1 protein in the 24h and 96 h treatment of Pt-ttpy at their respective IC₈₀ concentration. Also shown is a blot of tubulin as a loading control. Right: protein quantification of MT-CO1 protein by Image J. Data is represented by two independent experiments. Data represents two independent experiments with mean \pm SEM.

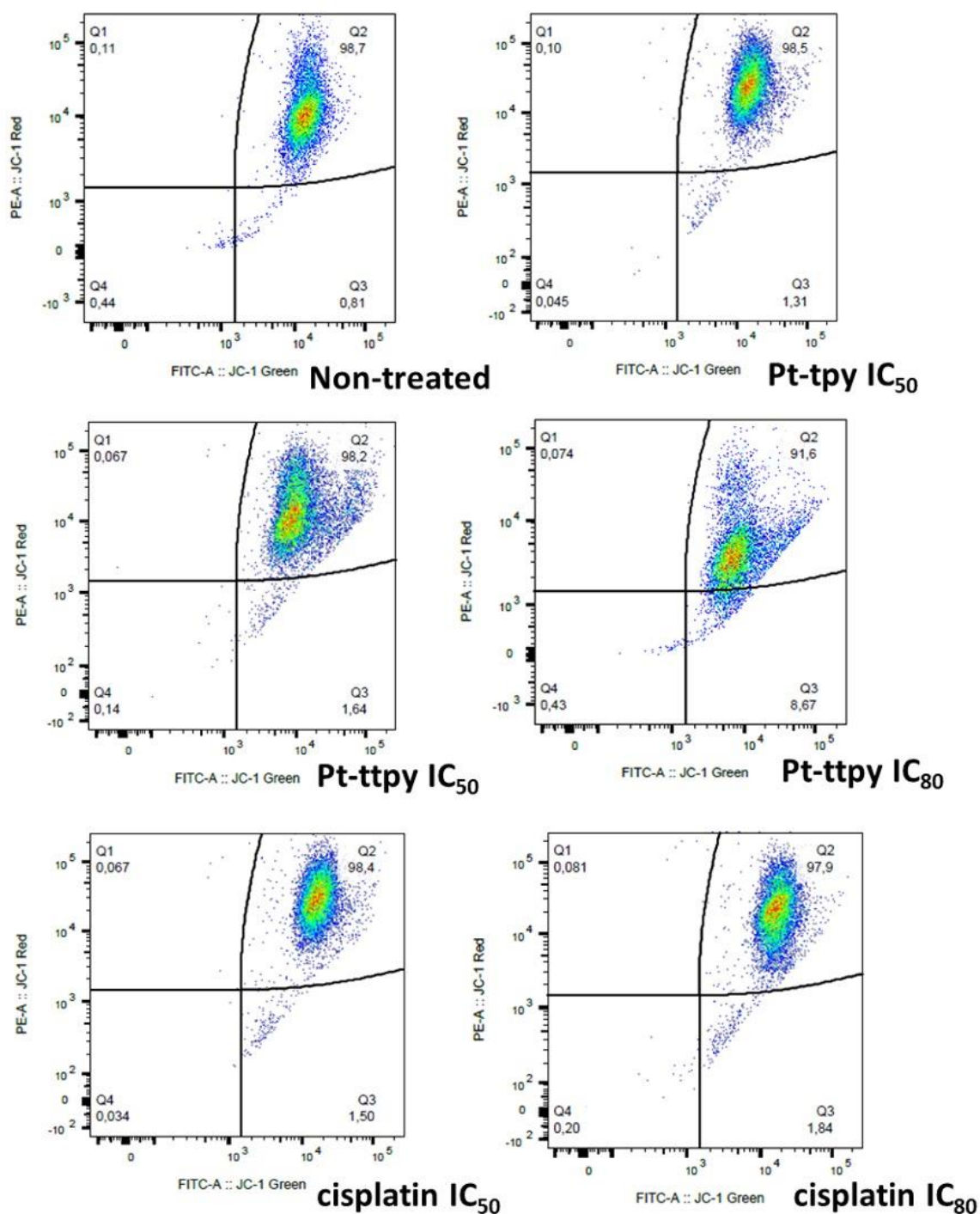


Fig. S4. Flow cytometry was used to quantify mitochondrial potential changes by the staining of JC1. Cell population in different quadrants with Q3 representing mitochondrial membrane potential loss (green monomer JC-1) in Pt-tpy, Pt-tpy and cisplatin treated cells at their IC₅₀ and IC₈₀ concentration for 96 hours in A2780 cells.

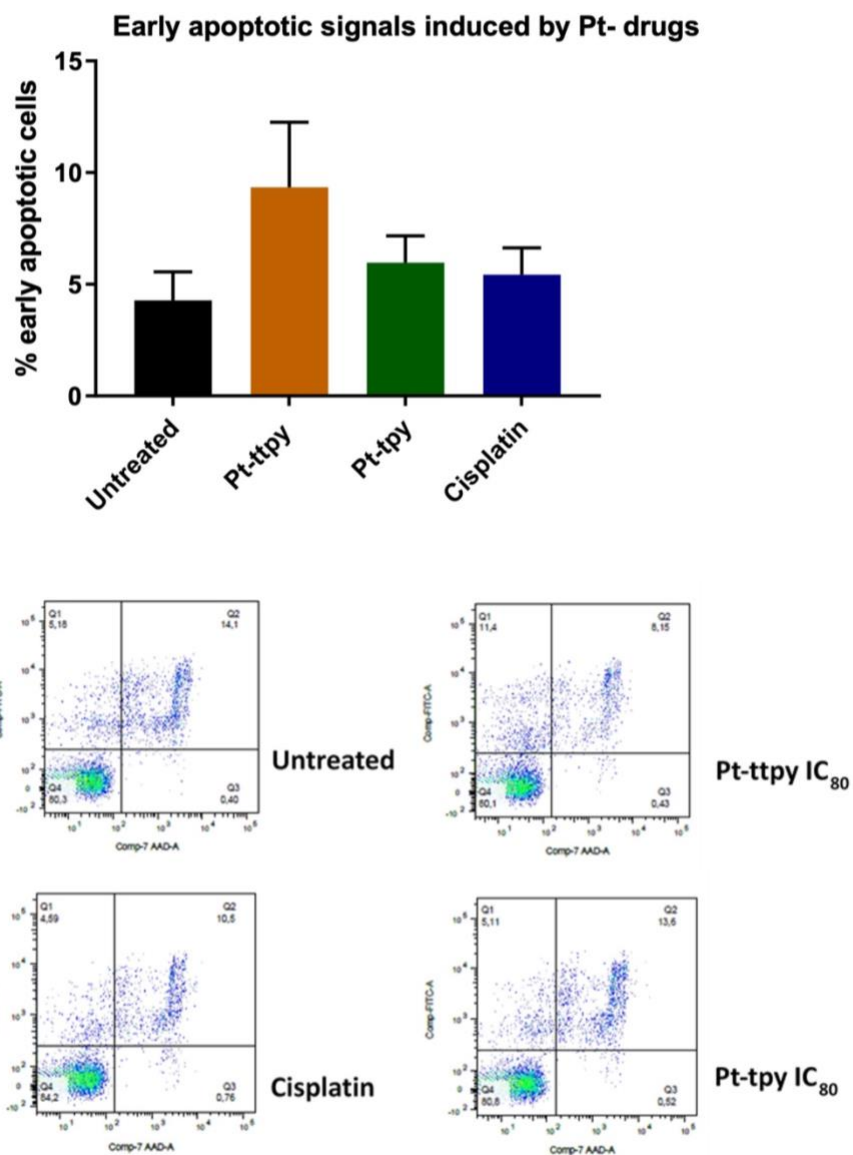


Fig. S5. Flow cytometry of the Annexin V apoptosis assay showing an increase of cells in Q1 (FITC+/7-AAD-) for early apoptosis after treatments with the three Pt complexes at their IC₈₀ concentration for 96h. Data are expressed as mean \pm SD of two biological replicates.

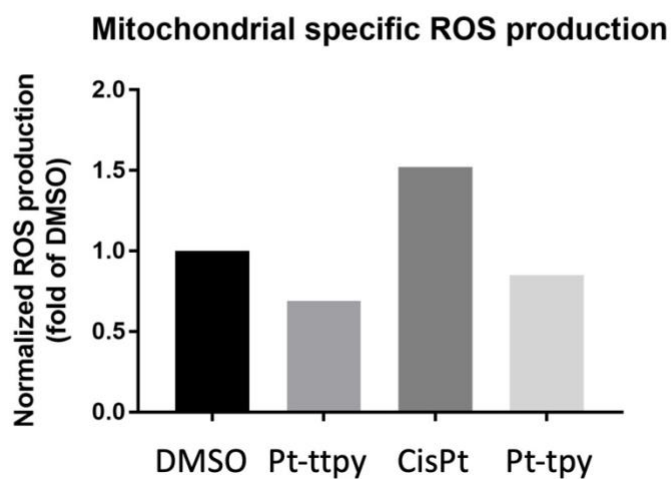
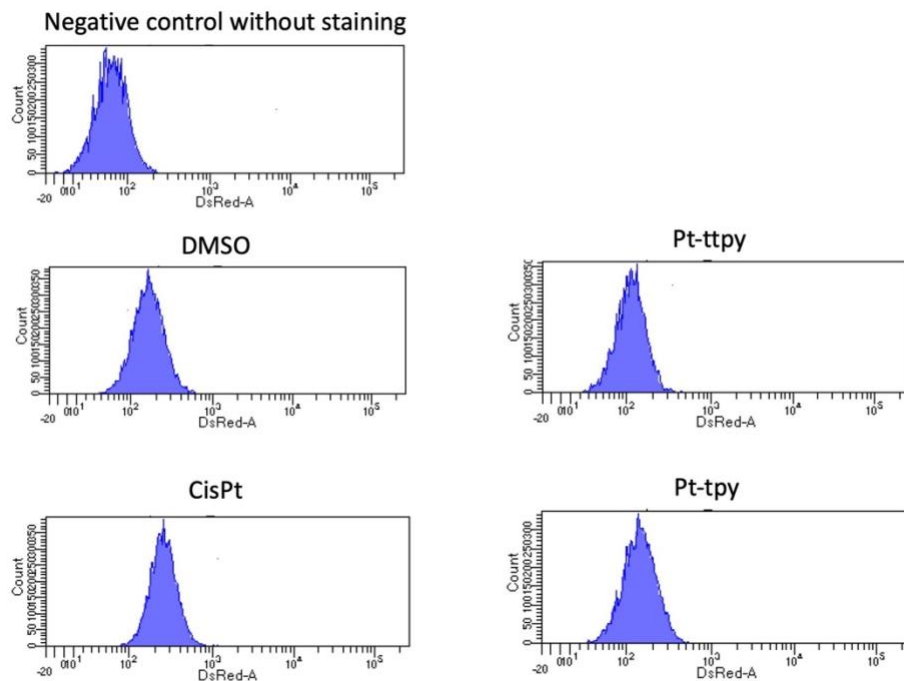


Fig. S6. Flow cytometry analysis of mitochondrial specific ROS production under the treatments of A2780 with the three Pt complexes. complexes (cisplatin, Pt-tpty and Pt-tpy) at their IC₈₀ con. for 96h.

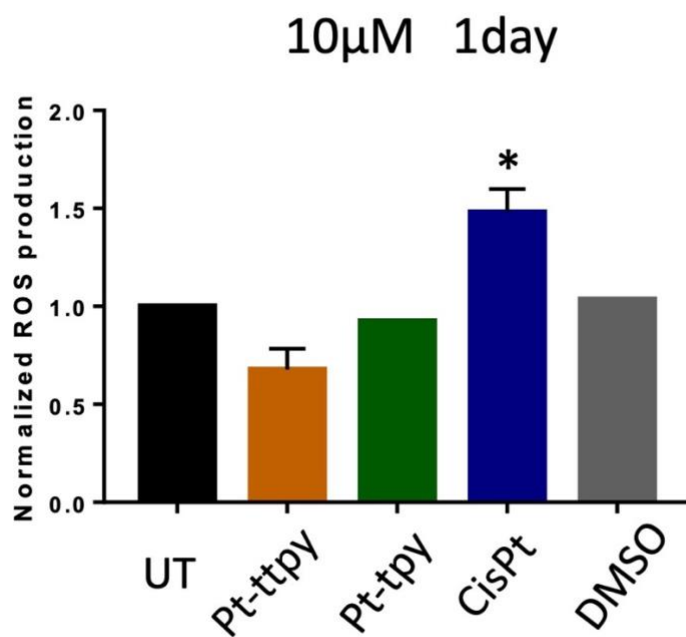


Fig. S7. Flow cytometry analysis of general ROS production under the treatments of A2780 with the three Pt complexes (cisplatin, Pt-ttpy and Pt-tpy) at 10 μ M con. for 24h. Data are expressed as mean \pm SEM of three biological replicates. P values were calculated by unpaired t-test: *P < 0.05.

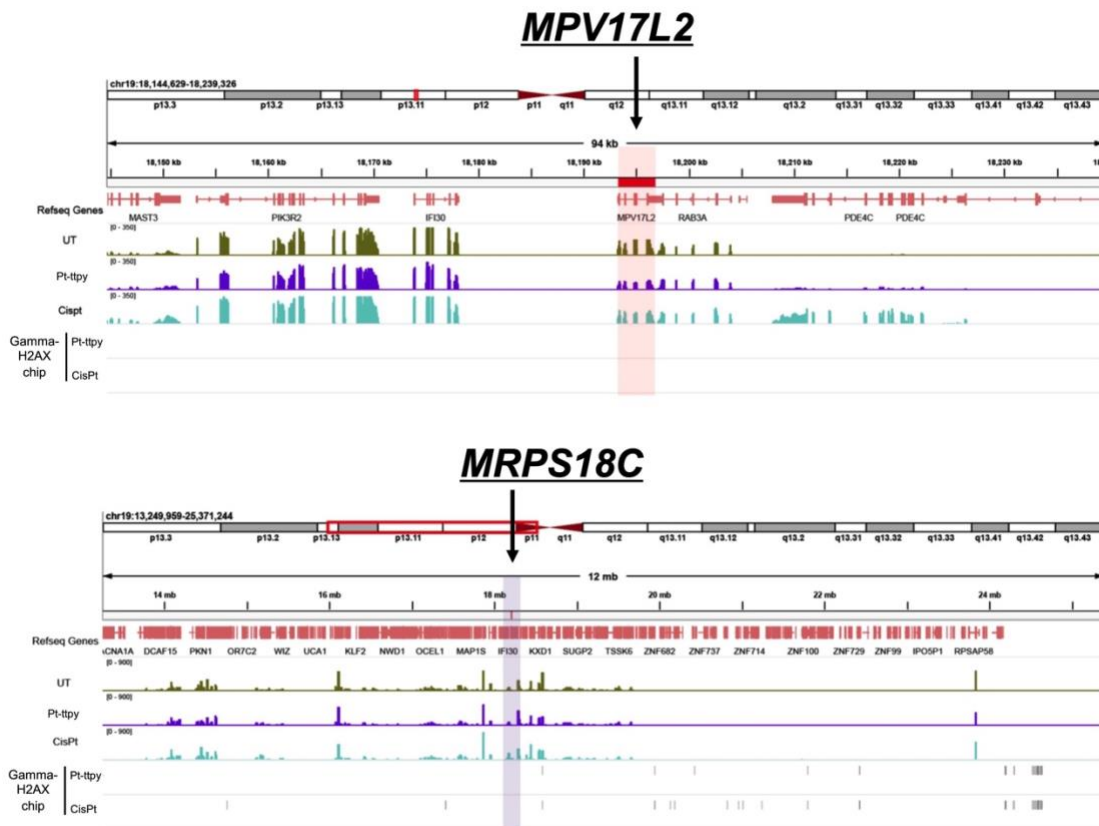


Fig. S8. IGV(2) showing the mt ribosome-related genes *MRPS18C* and *MPV17L2* expression, as well as the peak distribution of Pt-ttpt and cisplatin γ -H2AX IPs over the untreated γ -H2AX IP.

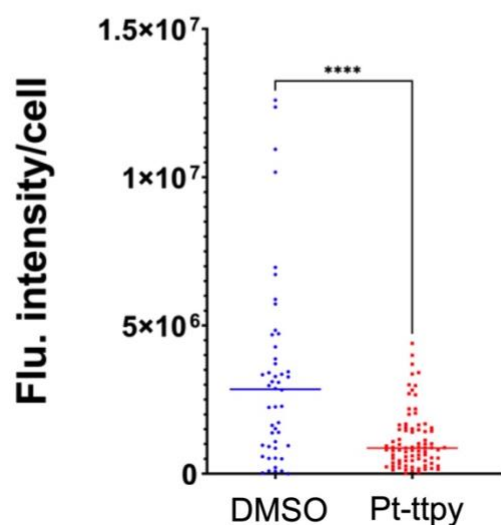
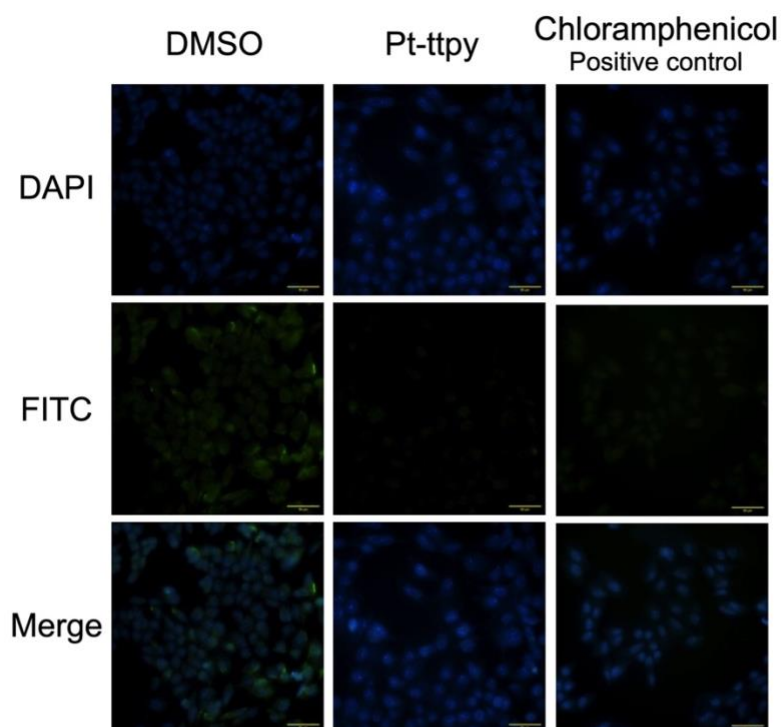


Fig. S9. UP: represented figures of fluorescent imaging of the mitochondria under Pt-ttpy and DMSO treatments in HeLa cells. A Positive control of blocking the synthesis of mitochondrial proteins by chloramphenicol was also presented. Down: Single-cell quantification showed Pt-ttpy significantly inhibited mitochondrial translation, DMSO group (>50), Pt-ttpy group (n>50). Data represents two independent experiments. P values were calculated toward the DMSO group: *P < 0.05, **P < 0.01, ****P < 0.0001, unpaired t-Student test.

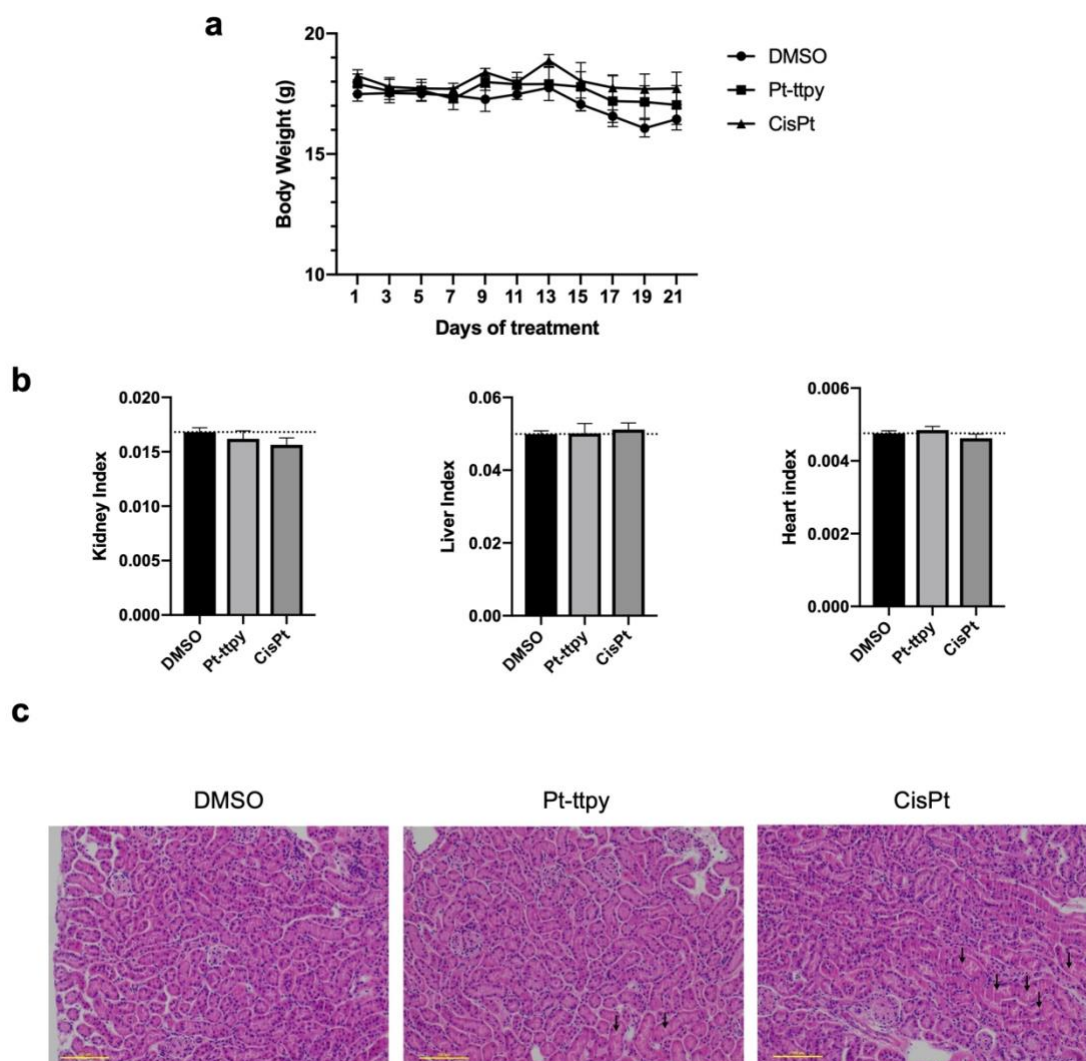


Fig. S10. cisplatin exhibited more toxicity to kidney, as compared with Pt-ttpy. (a) Body weight curve of mice under the treatments of DMSO, Pt-ttpy and cisplatin. (b) Index of the major tissues, including kidney, liver, and heart, post indicated treatments. Data is represented as mean \pm SEM. (c) The Pt-ttpy and cisplatin groups exhibited turbid staining, edema (\downarrow), indistinct intercellular boundaries, and uneven nuclear staining in the epithelial cells of renal proximal tubules, with the cisplatin group showing a more pronounced manifestation of these characteristics. The images are represented for three mice in each group.

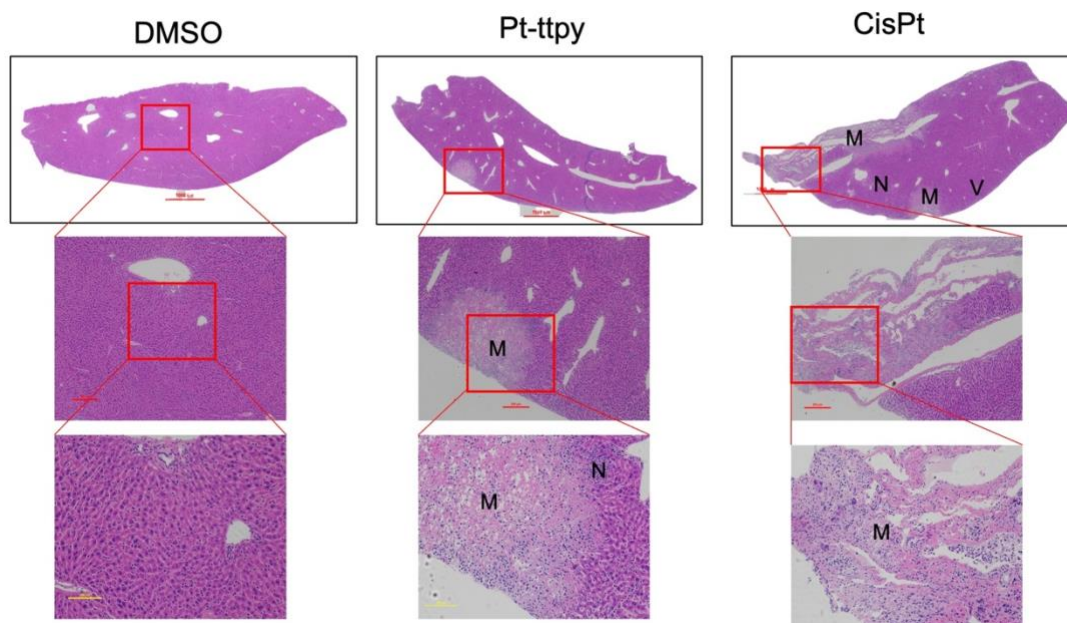


Fig. S11. cisplatin induced more toxicity to liver as compared with Pt-ttpy. Up: full scan of liver post indicated treatments. Down: Pt-ttpy induced neutrophil infiltration (N) in some areas without hepatocyte apoptosis, and cisplatin induced massive inflammation (I) around portal vein and blood vessels with enlarged sinusoidal space and vascular congestion (V). The images are represented for three mice in each group.

Table S1. A list of Primers for PCR

| Gene | Fw sequence (5'→3') | Rv sequence (5'→3') |
|----------------------|---------------------------|---------------------------|
| Actin | TCACCCACACTGTGCCCATCTACGA | CAGCGGAACCGCTCATTGCCAATGG |
| 12S | TAGCCCTAAACCTCAACAGT | TGCGCTTACTTTGTAGCCTTCAT |
| tRNA-Leu(UUR) | CACCCAAGAACAGGGTTTGT | TGGCCATGGGTATGTTGTTA |
| ND4 | TCTGTGCTAGTAACCACGTTT | AAAACCCGGTAATGATGTCG |
| COX III | CCACTCCTAAACACATCCGTA | GCCAATAATGACGTGAAGTCC |
| mt-deletion | TTCCTCATCACCCAATAAAAA | TTCGATGATGTGGTCTTTGG |
| COX I | AATAGGAGCTGTATTTGCCAT | AGAAAGTTAGATTTACGCCGAT |
| Cytb | TTATTGACTCCTAGCCGCAGA | TAGTACGGATGCTACTTGTCCA |
| ND6 | ATATACTACAGCGATGGCTA | AATCCTACCTCCATCGCTA |
| AURKAIP1 | GCAAAAACGTGCTGAAGATCCGC | GCCTCAGGTCTTTCTCGAACTTG |
| DHX30 | GAGCACTACCTAGAGGACATCC | CGATGTGCAGAACCAGATCAGTC |
| ERAL1 | CTGGACCACTTCCCTCGGATTCT | TCAGGGTGATGGACCAAGAGGA |
| GUF1 | GATTCCAGTGTGACCGTTCATCG | TTCTTGCTCCAGTCGCTGTTG |
| MPV17L2 | AGGGTCAGACAGTGGGTGAGAG | GCCGTTGATGTAGGTGACTCGA |
| MRM2 | GTGAACGAGAGGCACCAGATTC | CAAGCACGAAGCCAACAGGAGA |
| MRM3 | AAGAGTCTGGGCTTCGCTACGA | AGAGCGTCTGAAATGAGCCTGC |
| MRPL12 | CTACATCCAAGGCATCAACCTCG | GATCTTCTCCGCCTCAGCTTTG |
| MRPL15 | AGGTGTGACCATCCAGCCACTT | GCAGCAATAGCTAGTTCTGAAGC |
| MRPL18 | TGGCACAGAGATGCTTAGAGGC | CACACCACCTTCTGTGATGGCA |
| MRPL20 | TACAGCTGCTAGCCAGGAACATG | CAGATCCGCTAGGACTTTCTCTG |
| MRPL32 | GGTGTAGGAGAAGAAATCCGCAG | GCACACCTTTTCATAGCAGTAGG |
| MRPL36 | AGCAGTGCGCTCACTTCTCTCA | CCTCTTACCAGGTAACAGTCC |
| MRPL37 | ACAGACCTGGACTGTAACGAGG | CTCTGGCTTCAAACCAACTGGG |
| MRPL38 | TGTTCCACGGTGCCACCTTTGT | CTCTTCTGCCTCATAGGTCACC |
| MRPL41 | TCAAGCCCTACGTGAGCTACCT | AGGTTGTCAGGGTCAAAGGTAC |
| MRPL44 | TCCAGAAGGAGTTAGAGCGGCA | GGAAAAGTTTTCTGTAACCGATG |
| MRPL46 | CCTTCGAGGAACAGCTGAACGA | CGAGGTTACTCTCTGTCCGCAT |
| MRPL49 | CAGTTTGTGGAGCGCCTGTTAC | TTGTGCATCCGAGAGCGTCGTA |
| MRPL52 | GAGCTCCCAGACTGGTCATATG | CAGCGTCCATTTCTGTGACAG |
| MRPS11 | CCTTTGCTTCTGTGGCACAGA | GCCTTTCACCACAACCTCGGATG |
| MRPS18C | CAGGTATCCAGCAATGAGGACC | GCATCCAGTAAATGGAGAAACAAAC |
| MRPS30 | GGCTTTTGAGACAAAACCTGTGCTG | GGTCGAGTAACATCTGCTTCACT |
| MRPS5 | GAAGAGTGTTCTCGGCAATGGC | TACTGCTGGCTCATCAGGTGAC |
| MRPL43 | GAGGAGAGCATCCACTGCAA | CCTGGATGCTAGGGTTGTGCG |
| MRPS24 | TGAGGCAGTTGTCTCCACAC | ACACAACCTTTGAGGGCACA |
| MRPL27 | CGGACAGCCGTTACATCCTT | GCCTGATGACTTTCCACCGA |
| MRPS26 | GCTGGCCAAATCCAAGATCG | CTGGTAACGCTCCATCAGCA |
| MRPL34 | CACTGCGGATATGGCTGTCT | TGATACTCATTCCCAGGAGC |
| MRPL11 | AGGCGTTTCCATCAACCAGT | CTGCCACCTCTTTCCCTGTT |
| MPV17L2 ^① | CAGGCAGTAGTTTGCGACTC | TGCTGGGATGATGATAGGCG |

| | | |
|----------|-----------------------|------------------------|
| MPV17L2② | GCCACAGATCACATCCCTTCT | TGGTTGCCCTACGTATTTCCA |
| MPV17L2③ | CGGGACGTAACGCAATTCTT | TGACCAATAAAAGGCAGGCG |
| MPV17L2④ | GTTCCCTTGGTTCCTGAGGGC | AGCGTGTTAGTGACGAGCAG |
| MPV17L2⑤ | ACGCTGCTTAGTCCTTCACC | AGTCGGGTGTCGGGATCAAA |
| MRPS18C① | CTTAACTGCTGCGTGCACAA | TCGTTACCACTGTTAATCGGCA |
| MRPS18C② | CAAGTCCTCCGTACCTGGTC | GGACCTCCTACGTACATGC |
| MRPS18C③ | ACCGGAAGCACGCATAAACT | GCAGGTCACGTGAGGCTTAT |
| MRPS18C④ | TTGCTGTTTGCGGTGGTCTA | GCGCTACAATGGAGCATAGGA |
| MRPS18C⑤ | AAGGGACATTTCCAGAGTCGC | AAAGTAACAGACCCGTCCCAG |

SI References

1. O. Rothfuss, T. Gasser, N. Patenge, Analysis of differential DNA damage in the mitochondrial genome employing a semi-long run real-time PCR approach. *Nucleic Acids Res* **38**, e24 (2010).
2. J. T. Robinson, H. Thorvaldsdottir, D. Turner, J. P. Mesirov, igv.js: an embeddable JavaScript implementation of the Integrative Genomics Viewer (IGV). *Bioinformatics* **39** (2023).